

CHEBYSHEV ACCELERATED SUBSPACE EIGENsolver FOR PSEUDO-HERMITIAN HAMILTONIANS

EDOARDO DI NAPOLI*, CLÉMENT RICHEFORT*, AND XINZHE WU*

Abstract. Studying the optoelectronic structure of materials can require the computation of up to several thousands of the smallest eigenpairs of a pseudo-hermitian Hamiltonian. Iterative eigensolvers may be preferred over direct methods for this task since their complexity is a function of the desired fraction of the spectrum. In addition, they generally rely on highly optimized and scalable kernels such as matrix-vector multiplications that leverage the massive parallelism and the computational power of modern exascale systems. The *Chebyshev Accelerated Subspace iteration Eigensolver* (ChASE) is able to compute several thousands of the most extreme eigenpairs of dense hermitian matrices with proven scalability over massive parallel accelerated clusters [30]. This work presents an extension of ChASE to solve for a portion of the spectrum of pseudo-hermitian Hamiltonians as they appear in the treatment of excitonic materials. The new pseudo-hermitian solver achieves similar convergence and performance as the hermitian one. By exploiting the numerical structure and spectral properties of the Hamiltonian matrix, we propose an oblique variant of Rayleigh-Ritz projection featuring quadratic convergence of the Ritz-values with no explicit construction of the dual basis set. Additionally, we introduce a parallel implementation of the recursive matrix-product operation appearing in the Chebyshev filter with limited amount of global communications. Our development is supported by a full numerical analysis and experimental tests.

Key words. Pseudo-hermitian solver, Excitonic Hamiltonian, Bethe-Salpeter equation, Chebyshev filter, Oblique Rayleigh-Ritz, Quadratic convergence, GPU-enabled eigensolver

1. Introduction. The optical properties of materials under light stimulation are typically studied through the *Bethe-Salpeter Equation* (BSE) [2]. For numerical solution the BSE is expressed as an eigenvalue problem represented by an excitonic Hamiltonian. Such an Hamiltonian is of the form

$$(1.1) \quad H := \begin{bmatrix} A & B \\ -\bar{B} & -\bar{A} \end{bmatrix} \quad \text{with} \quad A = A^* \quad \text{and} \quad B = B^T.$$

The $m \times m$ dense blocks A and B are respectively referred to as resonant and coupling terms. The two blocks \bar{A} and \bar{B} simply stand for the conjugate of A and B . The Hamiltonian H is dense, has size $n := 2m$, and is termed a pseudo-hermitian matrix, as it satisfies the relation

$$(1.2) \quad SH = H^*S \quad \text{with} \quad S := \begin{bmatrix} I & 0 \\ 0 & -I \end{bmatrix}.$$

This paper focuses on the most common case in which the eigenproblem

$$(1.3) \quad H\mathbf{v} = \lambda\mathbf{v} \Leftrightarrow SH\mathbf{v} = \lambda S\mathbf{v} \quad \text{with} \quad \mathbf{v} \in \mathbb{C}^n \quad \text{and} \quad \lambda \in \mathbb{R}$$

is “definite”, meaning that SH is *hermitian positive definite* (HPD), i.e.,

$$(1.4) \quad SH = \begin{bmatrix} A & B \\ \bar{B} & \bar{A} \end{bmatrix} \succ 0.$$

We will further see that the eigenvalues λ in (1.3) are real-valued because of the positive-definiteness of SH . When the coupling-term B can be neglected, then the pseudo-hermitian eigenproblem reduces to an hermitian eigenvalue problem for which

*Jülich Supercomputing Centre, Forschungszentrum Jülich, Germany (e.di.napoli@fz-juelich.de, c.richefort@fz-juelich.de, xin.wu@fz-juelich.de)

the list of modern numerical libraries is comprehensive [4, 9, 12, 14, 27, 6]. However, this approximation is not always possible and can lead to inaccurate simulation of the desired optical properties of the materials. Therefore, developing fast and scalable eigensolvers for the original pseudo-hermitian eigenproblem could have a potential important impact in the community of materials scientists studying optoelectronics. While direct eigensolvers such as ELPA introduced variants for this case [19, 18], modern iterative eigensolvers cannot yet extract more than a few hundreds eigenpairs [1, 16]. In this paper, we present an expansion of the *Chebyshev Accelerated Subspace iteration Eigensolver* (ChASE) to compute several thousands of eigenpairs of pseudo-hermitian Hamiltonians with convergence and performance similar to the hermitian variant.

In the remaining of the paper, we give a concise state-of-the-art on eigensolvers for solving Hamiltonians arising from excitonic physics. Then, we introduce the standard workflow of ChASE in the hermitian case, and highlight each part that requires an extension to the pseudo-hermitian one. After deriving the numerical properties of the pseudo-hermitian Hamiltonians, we tackle the algorithmic upgrade for each independent component of ChASE, followed by a discussion on its parallel implementation. Finally, numerical tests are presented on large pseudo-hermitian matrices, including strong scaling experiments and parallel efficiency on massively parallel multi-GPU platforms.

1.1. State-of-the-art. Studying the optical properties and the electronic structure of materials has a strategical significance. In the perspective of improving energy production and storage, one important knowledge are the energies of quasiparticles called excitons, which can be extracted by solving the BSE [21], as in the Yambo code [15]. This step is done by computing a few of all the eigenvalues of the Hamiltonian matrix. The coupling term B is occasionally negligible, therefore the *Tamm-Dancoff Approximation* (TDA) [10] reduces the pseudo-hermitian eigenvalue problem to an hermitian one of the form

$$(1.5) \quad AX = X\Omega,$$

where X denotes a set of right eigenvectors of the hermitian resonant A and Ω the diagonal matrix whose entries contain their associated eigenvalues. Here, the eigenvalues on the diagonal of Ω are real, and the columns of X form an orthonormal set. When the full spectrum is required, a direct eigensolver of $\mathcal{O}(m^3)$ complexity must be applied. Direct eigensolvers for hermitian matrices have been extensively studied over the past decades, and several classical algorithms—including the QR algorithm, divide-and-conquer, and bisection with the inverse iteration—are now standard in the literature [5]. These algorithms provide robust and accurate solutions, but the Hamiltonian size grows extremely rapidly with the number of atoms in a system, creating significant computational and memory challenges. Efficient parallelization on modern large-scale distributed-memory computing platforms is therefore essential, also considering that big matrices cannot always fit on a shared memory platform ¹.

Several High-performance libraries targeting the full spectrum of hermitian matrices on distributed-memory machines have emerged, including ScaLAPACK [4], EigenEXA [12], SLATE [6], and ELPA [14]. Recently, cuSolverMp library introduced by NVIDIA,

¹A complex double precision dense matrix of size 100000 requires almost 150Gb.

as a production-level implementation of dense eigensolver on distributed-memory GPU platforms, has demonstrated the capability to compute millions of eigenvectors for matrices of size exceeding 10^6 on modern supercomputers [25].

When the full spectrum is not required and only a subset of eigenpairs is of interest, iterative methods of complexity $\mathcal{O}(m^2)$ provide a more suitable alternative. The SLEPc [9] library incorporates implementations of several iterative algorithms based on Lanczos or Krylov procedures. Meanwhile, filtered subspace iterative methods, such as the one implemented in ChASE [27], target the computation of eigenvectors associated with the most extreme eigenvalues by applying a Chebyshev polynomial filter at each iteration. From the filtered subspace, a Rayleigh-Quotient of small size is constructed, and the Ritz pairs are generally computed by performing its eigendecomposition with a divide-and-conquer algorithm. Compared to traditional Krylov approaches, ChASE exhibits several advantages on modern architectures, in particular GPUs: its reliance on dense matrix-matrix multiplications (GEMMs) allows for high efficiency on accelerator hardware, its block formulation naturally improves data locality, and the algorithm is well suited to exploit parallelism at scale [30].

While the TDA generally provides sufficiently accurate solutions to the BSE, it may become inaccurate or even physically inappropriate in certain cases [7, 17]. When the coupling term B cannot be neglected, the full eigenproblem is written

$$(1.6) \quad HV = V\Lambda,$$

where V is the set of right eigenvectors, each associated with an eigenvalue contained by the diagonal matrix Λ . Additionally, [23] demonstrates that, when condition (1.4) is satisfied, the eigenvalues Ω of matrix A provide an upper bound for the eigenvalues Λ of the full Hamiltonian H . Importantly, the resulting shift between Ω and Λ is generally non-negligible, indicating that the spectrum of A alone may not be sufficient for accurate simulations. Moreover, since H is twice as large as A due to the inclusion of the coupling term B , the computational cost of solving the full eigenproblem is substantially higher. This observation motivates the development of scalable eigensolvers for pseudo-hermitian matrices, achieving performance comparable to that of hermitian solvers, which can provide significant improvements for large-scale materials science simulations. In that direction, [23] proposed a method based on a direct eigensolver that exploits the pseudo-hermitian structure of H in (1.1). The approach solves the full eigenproblem (1.6) by computing the Cholesky factorization of a real symmetric positive definite (SPD) matrix that is spectrally equivalent to SH . The Cholesky factors are then recycled to construct a hermitian matrix sharing the same eigenvalues as the pseudo-hermitian Hamiltonian H , while the eigenvectors are recovered through back transformations. Two notable advantages of this method are that the spectral properties of the pseudo-hermitian matrix are preserved despite the backward error of the Cholesky factors, and that a standard direct hermitian eigensolver can be applied, bypassing the non-hermitian structure of H . A related approach was introduced in [19], where the eigendecomposition is instead carried out on a real skew-symmetric matrix, allowing the use of real arithmetic in the diagonalization step. This variant has been implemented in ELPA and has been shown to outperform the complex hermitian eigensolver in ScaLAPACK by a factor of 3. An extensive summary of direct eigensolvers for the BSE can be found in [18].

On the side of iterative eigensolvers for pseudo-hermitian matrices, a straightforward option is to apply general non-hermitian methods such as Lanczos or Arnoldi. However, these approaches are typically more expensive and fail to exploit the specific properties of H . To the best of our knowledge, the first Lanczos-based method tailored to the pseudo-hermitian Bethe-Salpeter Hamiltonian, with a computational cost comparable to the hermitian case, was introduced in [8]. A few years later, [22] enhances the stability of this algorithm, leading to improved convergence. Building upon these the foundations, [1, 16] present three variants of the thick-restarted Lanczos method [28] designed to compute a few hundred eigenpairs efficiently. Numerical experiments demonstrate promising performance in terms of scalability and convergence. Nevertheless, the authors acknowledge that extending these methods to compute a much larger portion of the spectrum—potentially several thousand eigenpairs—is challenging (see [1, Section 6]), because as more eigenpairs are computed, restarted Lanczos methods tend to lose orthogonality and become numerically unstable. This calls for alternative strategies, such as polynomial filtering techniques, which can selectively amplify the desired spectral intervals, leading to faster convergence and improved numerical stability, and exploits high-performance computing through GEMMs and parallelism. This is exactly the approach adopted in ChASE.

Precisely, the goal of this work is to extend ChASE to pseudo-hermitian Hamiltonians in order to achieve fast and scalable convergence for the computation of several thousand eigenpairs. In Section 2, we start by recalling the classical workflow of ChASE. Section 3 then examines the spectral properties of the pseudo-hermitian Hamiltonian to identify the components that require modification. The corresponding algorithmic developments are addressed in Section 4, including parameter estimation in the setup phase and the construction of the Rayleigh–Quotient. In particular, we prove in Section 5 that our oblique variant of the Rayleigh–Ritz method enables quadratic convergence of the Ritz-values, mirroring the hermitian case. After introducing the parallel implementation in Section 6, Section 7 reports convergence and strong scaling experiments performed on large GPU platforms and on different sized pseudo-hermitian Hamiltonians. These results demonstrate that ChASE can be successfully generalized to the pseudo-hermitian setting while preserving both efficiency and scalability.

2. ChASE for hermitian matrices. The standard ChASE algorithm computes the `nev` smallest eigenvalues of the hermitian matrix A in (1.5), with their associated eigenvectors. Its two main components are: (i) a well designed Chebyshev polynomial that filters the external eigenvectors, and (ii) a Rayleigh–Ritz procedure that extracts approximations of the eigenpairs from the orthonormalized filtered subspace. Let ω_i denote the i th smallest eigenvalue of A . While ChASE targets the interval $[\omega_1, \omega_{\text{nev}}]$, the filter is constructed over the slightly enlarged interval $[\omega_1, \omega_{\text{nev}+\text{nex}}]$ using a Chebyshev polynomial of degree `deg`. This enlargement increases the rank of the search space to $\text{nevex} := \text{nev} + \text{nex}$, which improves the accuracy of the filter near ω_{nev} and accelerates convergence. Conversely, increasing `deg` enhances the damping of unwanted eigenvectors by flattening the polynomial p near zero on the complement interval $[\omega_{\text{nevex}}, \omega_m]$, where $\omega_{\text{nevex}} = \omega_{\text{nev}+\text{nex}}$. The effectiveness of this approach depends on accurate estimates of the spectral bounds $\omega_1, \omega_{\text{nevex}}$ and ω_m , which are respectively approximated by the parameters $\mu_1, \mu_{\text{nevex}}$ and μ_m obtained from a few Lanczos iterations (25 is the default value). The extreme parameters μ_1 and μ_m are taken as the smallest and largest approximated eigenvalues from Lanczos iterations,

respectively. Meanwhile, μ_{nevex} is estimated by integrating an approximation of the spectral density function [13], so that the interval $[\mu_1, \mu_{\text{nevex}}]$ covers nevex/m of the spectral weight. The resulting polynomial filter is illustrated in Figure 2.1.

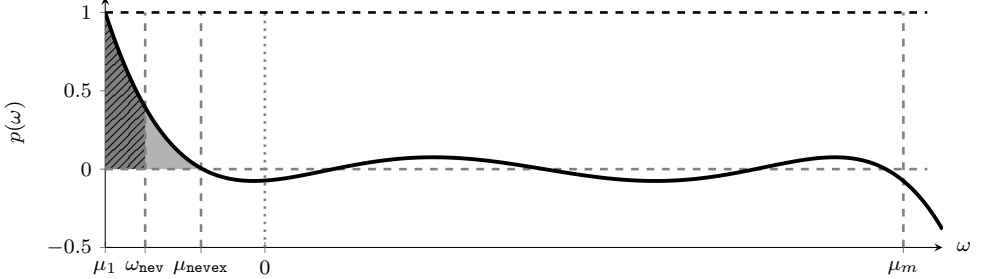


Fig. 2.1: Illustration of the effect of the Chebyshev polynomial filter - the gray filling corresponds to the filtered area and the dashed pattern represents the area of target eigenpairs.

Once the polynomial filter is designed, the search space \hat{V} is initialized with random vectors drawn from a normal distribution and then enters the main loop. At each iteration, \hat{V} is filtered and subsequently orthonormalized using either a distributed Cholesky QR or a block Householder QR algorithm, depending on its conditioning. In both cases, the orthonormalized vectors are collected in the $m \times \text{nevex}$ matrix Q . ChASE then proceeds with the Rayleigh-Ritz procedure to compute approximate eigenpairs. Specifically, a Ritz pair $(\tilde{\omega}, \tilde{\mathbf{x}})$ approximates an exact eigenpair (ω, \mathbf{x}) , where $\tilde{\omega} \in \mathbb{R}$ and $\tilde{\mathbf{x}} \in \text{range}(Q)$. Here, ω is an eigenvalue in the diagonal matrix Ω of (1.5), and \mathbf{x} is an eigenvector from the set X . Each Ritz-pair should satisfy the following Galerkin condition (see e.g. [20])

$$(2.1) \quad \tilde{\mathbf{y}}^* (A\tilde{\mathbf{x}} - \tilde{\omega}\tilde{\mathbf{x}}) = 0, \quad \forall \tilde{\mathbf{y}} \in \text{range}(Q).$$

The orthonormal basis Q defines the hermitian Rayleigh-Quotient $G := Q^*AQ$, from which the Ritz pairs are obtained by solving the reduced problem $GZ = Z\tilde{\Omega}$. The Ritz values are given directly by the diagonal entries of $\tilde{\Omega}$, while the corresponding Ritz vectors \tilde{X} are recovered as $\tilde{X} := QZ$, so that each $\tilde{\mathbf{x}}$ is a column of \tilde{X} . In the hermitian case, Cauchy's interlace theorem guarantees that the eigenvalues of G interlace with those of A , which facilitates locating the Ritz values $\tilde{\Omega}$. Moreover, an approximate eigenvector $\tilde{\mathbf{x}}$ be decomposed as the linear combination $\tilde{\mathbf{x}} = \gamma\mathbf{x} + \sigma\mathbf{e}$, where \mathbf{x} is the target eigenvector and $\mathbf{e} \perp \mathbf{x}$. In the hermitian case, a key property established in [24] is that the orthogonal Rayleigh-Ritz procedure converges quadratically with respect to σ , in the sense that

$$(2.2) \quad |\omega - \tilde{\omega}| \leq \mathcal{O}(\sigma^2).$$

This quadratic convergence is central to the efficiency of ChASE, as it ensures the extremely rapid convergence of Ritz values with sufficiently accurate filtered subspace. In Section 4.3, dedicated to Rayleigh-Ritz procedure, we demonstrate that this desirable quadratic convergence can be replicated in the pseudo-hermitian case. Preserving this feature is a cornerstone for achieving fast convergence. The final step of each iteration then consists of computing the residuals $\mathbf{r}_i := \|A\tilde{X}_{:,i} - \tilde{\omega}_i\tilde{X}_{:,i}\|_2$

and locking each Ritz vector $\tilde{X}_{:,i}$ that satisfies $r_i \leq \text{tol}$, where tol is a prescribed input tolerance. The number of locked vectors locked is incremented accordingly. The iteration proceeds until all nev desired smallest eigenvalues are locked or the prescribed maximal number of iterations is reached (i.e., $\text{locked} = \text{nev}$). For what follows, define $k := \text{nevex} - \text{locked}$ the number of non-converged eigenvectors. Each new iteration reuses the non-locked columns of \tilde{X} to form a reduced search space \hat{V} of size k , which is re-orthonormalized against the locked vectors to preserve orthogonality. The standard workflow for hermitian matrices is summarized in Algorithm 2.1, while details of the locking strategy are discussed in [27].

Algorithm 2.1 Standard workflow of ChASE for hermitian matrices

Input: hermitian matrix A of size $m \times m$, nev , and nex

Output: $(\Omega_{\text{nev}}, X_{\text{nev}})$ with $\Omega_{\text{nev}} = \text{diag}(\omega_1, \dots, \omega_{\text{nev}})$ and $X_{\text{nev}} = [\mathbf{x}_1, \dots, \mathbf{x}_{\text{nev}}]$

- 1: $\hat{V} \leftarrow \text{randn}(m, \text{nevex})$
 - 2: Estimate $\omega_1, \omega_{\text{nevex}}$ and ω_m with Lanczos
 - 3: **while** $\text{locked} < \text{nev}$ **do**
 - 4: Filter the vectors, $\hat{V} \leftarrow p(A)\hat{V}$
 - 5: Orthonormalize $Q \leftarrow [Y, \hat{V}]R^{-1}$
 - 6: Select non-locked space only $Q \leftarrow Q_{:, \text{locked}: \text{nevex}}$
 - 7: Compute Rayleigh quotient $G \leftarrow Q^*AQ$
 - 8: Solve the reduced problem $GZ = Z\tilde{\Omega}$
 - 9: Compute $\hat{V} \leftarrow QZ$
 - 10: Compute the residuals $\text{Res}(\tilde{\Omega}, \hat{V})$
 - 11: Lock the converged eigenpairs $(\Omega, \tilde{X}, \hat{V}) \leftarrow \text{Locking}(\tilde{\Omega}, \hat{V})$
 - 12: $\text{locked} \leftarrow \text{size}(\tilde{X})$
 - 13: **end while**
 - 14: $\Omega_{\text{nev}}, X_{\text{nev}} \leftarrow \Omega, \tilde{X}$
-

3. Properties of pseudo-hermitian Hamiltonians. In this section, we recall the main properties of pseudo-hermitian Hamiltonians to identify which components of ChASE require modification. Let \mathbf{u} and \mathbf{v} denote respectively the left and right eigenvectors associated with the eigenvalue λ of H , such that

$$(3.1) \quad \mathbf{u}^* H = \lambda \mathbf{u}^* \quad \text{and} \quad H \mathbf{v} = \lambda \mathbf{v}.$$

3.1. General pseudo-hermitian Hamiltonians. We first consider the general case where the positivity (1.4) of SH is not assumed, which allows us to naturally extend these properties to H needed for ChASE when the positivity of SH holds.

It is well known that the eigenvalues of a pseudo-hermitian Hamiltonian come in quadruplets (see [3, Theorem 1]). Specifically, if λ is an eigenvalue of H , then $\{\lambda, \bar{\lambda}, -\lambda, -\bar{\lambda}\}$ also belong to the spectrum, whose associated eigenvectors satisfy the following theorem.

THEOREM 3.1. *The quadruplet $\{\lambda, \bar{\lambda}, -\lambda, -\bar{\lambda}\}$ belongs to the spectrum of H , with*

$$(3.2) \quad HS\mathbf{u} = \bar{\lambda}S\mathbf{u} \quad , \quad HJ\bar{\mathbf{u}} = -\lambda J\bar{\mathbf{u}} \quad , \quad HK\bar{\mathbf{v}} = -\bar{\lambda}K\bar{\mathbf{v}},$$

where K and J are defined as follows

$$(3.3) \quad K := \begin{bmatrix} 0 & I \\ I & 0 \end{bmatrix} \quad \text{and} \quad J := \begin{bmatrix} 0 & I \\ -I & 0 \end{bmatrix}.$$

An important implication of Theorem 3.1 is that one can deduce the most extreme positive eigenpairs from the most negative ones, and vice-versa. Therefore, computing half eigenpairs is sufficient to recover the entire spectrum.

The next theorem identifies bounds on the location of the eigenvalues in the complex plane, with respect to the blocks A and B . The eigenvalues with the limits of the field of values are illustrated in Figure 3.1a.

THEOREM 3.2. *Let A and B denote the block components of H as in (1.1), then the spectrum of H is enclosed within a finite plane such that*

$$(3.4) \quad \operatorname{Re}(\lambda) \in [-\rho(A), \rho(A)] \quad \text{and} \quad \operatorname{Im}(\lambda) \in \left[-\sqrt{\rho(B^*B)}, \sqrt{\rho(B^*B)} \right],$$

where $\rho(\cdot)$ denotes the spectral radius.

Proof. See the proof in Appendix A. □

3.2. The definite eigenvalue problem. In the target case where the condition (1.4) holds, the eigenvalues of H are real. Theorem 3.3 also establishes a direct link between the left and right eigenvectors via the matrix S defined in (1.2).

THEOREM 3.3. *If SH is HPD, then the eigenvalues of H are real, and the left and right eigenvectors are related by*

$$(3.5) \quad \lambda = \bar{\lambda} \quad \Leftrightarrow \quad \mathbf{u} = S\mathbf{v}.$$

Proof. Since SH is HPD, it admits a Cholesky factorization $SH = LL^*$ with L lower triangular factor. The eigenvalue problem (3.1) can then be written as

$$(3.6) \quad SSH\mathbf{v} = \lambda\mathbf{v},$$

which is equivalent to the hermitian eigenvalue problem

$$(3.7) \quad L^*SL\mathbf{y} = \lambda\mathbf{y}, \quad \mathbf{y} = L^*\mathbf{v}.$$

Hence, λ is real, i.e., $\lambda = \bar{\lambda}$. Furthermore, from Theorem 3.1 we know that $HS\mathbf{u} = \lambda S\mathbf{u}$. Identifying with $H\mathbf{v} = \bar{\lambda}\mathbf{v}$ yields $S\mathbf{u} = \mathbf{v}$. □

Theorem 3.3 has two immediate consequences. First, the left eigenvectors are obtained from the right ones by the action of S . Since S has the block-diagonal structure prescribed by (1.2), this amounts to flipping the sign of the lower block of each right eigenvector. Explicit computation of left eigenvectors is therefore unnecessary: they can be deduced at negligible cost from the right eigenvectors. Second, all eigenvalues lie on the real axis, within the field of values characterized in Theorem 3.2. Their magnitude is bounded by the spectral radius of A , as stated in Lemma 3.4. This conclusion is consistent with [23, Theorem 4] which demonstrates that the eigenvalues of A provides an upper bound for the positive eigenvalues of H .

LEMMA 3.4. *If SH is HPD, then λ , the eigenvalues of H , satisfy*

$$(3.8) \quad \lambda \in [-\rho(A), \rho(A)].$$

Moreover, since A is a principal block of the HPD matrix SH , it is itself HPD. The eigenvalue distribution of the Hamiltonian H is illustrated in Figure 3.1b.

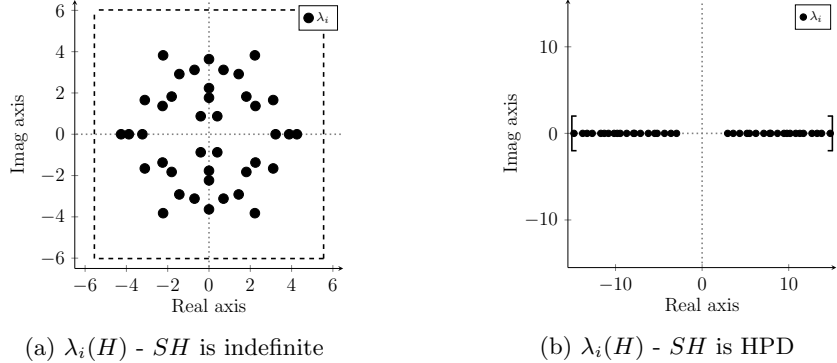


Fig. 3.1: Eigenvalues of H when SH is indefinite vs. HPD - The brackets and the dashed square represent the bounds of the fields of values $\mathcal{F}(H)$

In what follows, let

$$(3.9) \quad U := [\mathbf{u}_1, \dots, \mathbf{u}_n], \quad V := [\mathbf{v}_1, \dots, \mathbf{v}_n]$$

denote respectively the set of left and right normalized eigenvectors, where each \mathbf{u}_i and \mathbf{v}_i is the left and right eigenvector corresponding to the i th eigenvalue λ_i .

Since H is non-hermitian, neither U or V is orthonormal. Instead, they satisfy a bi-orthogonality relation, that the scalar product $d_{ij} := \mathbf{u}_i^* \mathbf{v}_j$ is zero only if $i \neq j$. Using the relation $U = SV$ introduced in Theorem 3.3, we obtain

$$(3.10) \quad D := V^* SV \quad \Rightarrow \quad H = V \Lambda D^{-1} V^* S,$$

where D is a diagonal matrix containing the non-zero entries d_{ii} on its diagonal. Hence, D is always full rank and invertible. To conclude this section, we show that the condition number of H equals the condition number of SH . This information will be useful for further theoretical developments.

THEOREM 3.5. *If SH is HPD,*

$$(3.11) \quad \text{cond}(SH) = \text{cond}(H).$$

Proof. Let $H = K \Sigma P^*$ be the singular value decomposition of H . Then, from the definition of a pseudo-hermitian matrix (1.2), we have $H^* = SHS = SK\Sigma P^* S$. Subsequently, it follows that $K = SP$. Substituting this into the singular value decomposition of H gives

$$(3.12) \quad SH = P \Sigma P^*,$$

which is the eigendecomposition of SH . Hence, the condition number of H and SH satisfy

$$(3.13) \quad \text{cond}(SH) = \frac{\lambda_{\max}(SH)}{\lambda_{\min}(SH)} = \frac{\sigma_{\max}(H)}{\sigma_{\min}(H)} = \text{cond}(H). \quad \square$$

In summary, when SH is HPD, the algorithm can leverage on the following properties:

- The eigenvalues of H are real, the same as the hermitian case, and appear as negative-positive pairs.
- The left eigenvectors follow directly from the right ones through the action of S , which simply flips the sign of their lower half block.
- The right eigenvectors themselves are not orthonormal, but instead form a bi-orthogonal system with respect to S .

These properties form the foundation for extending the ChASE framework to pseudo-hermitian problems, as detailed in the next section.

4. Extending ChASE to pseudo-hermitian Hamiltonians. The hermiticity of the matrix is a central assumption in the current design of ChASE. To extend the framework to pseudo-hermitian eigenproblems such as (1.6), three major components of the algorithm must be revised. *First, Spectral bounds estimation.* The estimation of λ_1 , λ_{nevex} , and λ_n (Line 2 in Algorithm 2.1) is no longer based on standard hermitian Lanczos algorithm. Instead, we employ a few iterations of the pseudo-hermitian Lanczos variant developed in [8]. Details are given in Section 4.1. While the Chebyshev filter (Line 4) still applies due to the real spectrum of H (Theorem 3.3), minor adjustments in the parallel matrix-matrix products are required to account for the pseudo-hermitian structure. This is discussed in Section 6. *Second, orthonormalization and locking of right eigenvectors.* The next step after filtering the target eigenvectors associated with smallest eigenvalues is to extract the locked eigenvectors from the current search space (Lines 5–6 in Algorithm 2.1). In the pseudo-hermitian case, the right eigenvectors are not orthonormal, meaning that the target vectors may remain correlated. As a result, orthonormalizing the locked columns against the remaining search space can impair convergence. Remedies for this issue are discussed in Section 4.2. *Third, Rayleigh-Ritz procedure.* Constructing the Rayleigh quotient G from a single orthonormal basis (Line 7) is effective in the hermitian case but performs poorly in the pseudo-hermitian setting. Instead, we adopt an oblique Rayleigh–Ritz scheme (Section 4.3). Section 5 will show that it achieves quadratic convergence of the Ritz values and allows forming G directly without explicitly constructing the dual basis.

4.1. Estimating λ_1 , λ_{nevex} and λ_n . We indicate with μ_1 , μ_{nevex} and μ_n the estimates of eigenvalues λ_1 , λ_{nevex} and λ_n of H . These estimates provide initial spectral bounds for the filtering and iteration steps, which relies on a few Lanczos iterations that must be adapted for the pseudo-hermitian case. One simple approach, proposed in [8], is to flip the sign of the lower part of the vectors after matrix-vector product to emulate the multiplication by the S matrix in (1.2). More advanced variants [1, 16] improve numerical stability, but since our Lanczos stage only generates rough eigenvalue estimates, we adopt the simpler method [8]. Moreover, in some cases, it may be beneficial to slightly overestimate the magnitude of λ_{nevex} and λ_n thereby widening the filtering interval and ensuring that undesired eigenvectors are sufficiently damped.

In addition, the eigenvalues of H are real and occur in symmetric opposite (positive–negative) pairs with respect to the zero (Figure 3.1b). To preserve the symmetry in the spectral density, we use an even number of Lanczos iteration, set $\mu_n = -\mu_1$, and integrate the spectral density over the negative axis only to determine μ_{nevex} .

During ChASE iterations, μ_{nevex} is updated from the largest non-converged Ritz values. This gradually narrows the filtering interval, focusing the search space on the target portion of the spectrum. An alternative strategy could use a power method

to estimate λ_1 and set $\mu_{\text{nevex}} = 0.0$ initially, letting these values adjust during iterations. However, since the computational cost is dominated by the Chebyshev filter and the Rayleigh-Ritz procedure, investing slightly more in the initial Lanczos setup is preferable, as it improves the starting interval and can reduce the total number of iterations. This is the approach adopted here.

4.2. Orthonormalization and locking. In the orthogonal Rayleigh–Ritz variant, the orthonormality of the search space Q is required. Although we adopt the oblique variant for pseudo-hermitian problems, orthonormality remains important for constructing the dual basis. In ChASE for the hermitian case, the search space is not only orthonormalized, but also orthonormalized against all already converged eigenvectors. This improves convergence by removing the information that has already been processed. However, this strategy only applies to hermitian matrices, where eigenvectors are orthonormal. In the general non-hermitian case, removing converged vectors from the search space can be counterproductive: because the target vectors may correlate with the converged ones, such removal can prevent convergence and cause stagnation.

For the pseudo-hermitian Hamiltonians we consider, Eq. (3.10) indicates that the right eigenvectors V are orthogonal to SV . Therefore, the converged eigenvectors, after flipping the sign of their lower parts, are irrelevant to the remaining non-converged vectors. To preserve convergence, the remaining search space should be orthonormalized against these sign-flipped locked eigenvectors. The only computational overhead compared to the hermitian orthonormalization step is one flip-sign operation performed at each iteration on the set of locked vectors. Line 5 of Algorithm 2.1 simply becomes

$$(4.1) \quad Q \leftarrow [SY, \hat{V}]R^{-1}.$$

4.3. The Rayleigh-Ritz Procedure. The Rayleigh-Ritz step is among the two most crucial components of ChASE. Chebyshev polynomial filter constructs a search-space Q , from which the Rayleigh-Ritz procedure extracts the “best” approximate eigenpairs of H . The precise definition of “best” depends on either the *Galerkin* (2.1) condition (orthogonal projection) or the more general *Petrov-Galerkin* (4.4) condition (oblique projection) is used.

Let $(\tilde{\lambda}, \tilde{\mathbf{u}}, \tilde{\mathbf{v}})$ denote an approximate eigen-triplet associated with the exact eigen-components $(\lambda, \mathbf{u}, \mathbf{v})$ corresponding to the eigenvalue, the left-eigenvector and right-eigenvector, respectively. In practice, left eigenvectors are not explicitly computed during the iteration, since they can be recovered *a posteriori* from the right eigenvectors via the relation (3.5). That said, the left eigenvectors, like the right ones, play a crucial role in the analysis of convergence.

We assume that all the eigenvectors along with their approximations are normalized, such that

$$(4.2) \quad \|\mathbf{u}\|_2 = \|\mathbf{v}\|_2 = \|\tilde{\mathbf{u}}\|_2 = \|\tilde{\mathbf{v}}\|_2 = 1, \quad \delta := \mathbf{u}^* \mathbf{v}, \quad \tilde{\delta} := \tilde{\mathbf{u}}^* \tilde{\mathbf{v}}.$$

Additionally, both $\tilde{\mathbf{u}}$ and $\tilde{\mathbf{v}}$ can respectively be decomposed as

$$(4.3) \quad \tilde{\mathbf{u}} = \gamma_{\mathbf{u}} \mathbf{u} + \sigma_{\mathbf{u}} \mathbf{e}_{\mathbf{u}}, \quad \tilde{\mathbf{v}} = \gamma_{\mathbf{v}} \mathbf{v} + \sigma_{\mathbf{v}} \mathbf{e}_{\mathbf{v}} \quad \text{with} \quad \mathbf{e}_{\mathbf{u}} \perp \mathbf{u} \quad \text{and} \quad \mathbf{e}_{\mathbf{v}} \perp \mathbf{v}.$$

For hermitian matrices, the orthogonal Rayleigh–Ritz variant guarantees quadratic convergence of Ritz values toward the exact eigenvalues. This guarantee is tied directly to the orthogonality of eigenvectors and the variational characterization of Ritz values. However, in the non-hermitian or pseudo-hermitian setting, these properties break down, and quadratic convergence is no longer ensured. Two key obstacles are:

- *Loss of orthogonality of right eigenvectors.* In the hermitian case, eigenvectors form an orthonormal basis, and the Rayleigh quotient provides tight error bounds. For pseudo-hermitian problems, or more generally non-hermitian problems, right eigenvectors can be highly non-orthogonal, or even nearly linearly dependent, which invalidates the quadratic error rule of (2.2). This loss of orthogonality amplifies sensitivity to perturbations and can lead to only linear convergence or even stagnation of Ritz values.
- *Asymmetry between left and right invariant subspace.* Even when the trial subspace Q approximates the right invariant subspace well, convergence of Ritz values also depends on how accurately the corresponding left invariant subspace is represented. Orthogonal Rayleigh–Ritz, which only enforces orthogonality with respect to Q , does not account for this dual structure. As a result, residuals can remain large in the dual sense, and the approximation may fail to capture the correct bi-orthogonal relationship between left and right eigenvectors.

These limitations motivate the introduction of the oblique Rayleigh–Ritz variants, which employs a dual basis $Q_{\mathcal{L}}$ satisfying the bi-orthogonality relation $Q_{\mathcal{L}}^*Q = I_k$, where we remind that $k := \text{never} - \text{locked}$. In this case, approximate eigenpairs satisfies the *Petrov–Galerkin* condition

$$(4.4) \quad \tilde{\mathbf{u}}^* \left(H\tilde{\mathbf{v}} - \tilde{\lambda}\tilde{\mathbf{v}} \right) = 0, \quad \text{with } \tilde{\mathbf{v}} \in \text{range}(Q) \quad \text{and} \quad \forall \tilde{\mathbf{u}} \in \text{range}(Q_{\mathcal{L}}),$$

which explicitly enforces that the residuals are orthogonal to the dual subspace (see e.g., [20]). This orthogonality is crucial because it decouples the errors of different approximate eigenpairs along the directions of the left eigenvectors, reducing cross-term contamination and enabling faster convergence. Here the subscript “ \mathcal{L} ” emphasizes that the range of $Q_{\mathcal{L}}$ should approximate the left invariant subspace.

The Rayleigh–Quotient is computed via the dual basis

$$(4.5) \quad G := Q_{\mathcal{L}}^*HQ.$$

Although we do not compute left eigenvectors in practice, they can in principle be obtained by back-transformations after computing the eigendecomposition of G

$$(4.6) \quad \tilde{\mathbf{v}} = Q\mathbf{w} \quad \text{with} \quad G\mathbf{w} = \tilde{\lambda}\mathbf{w}, \quad \text{and} \quad \tilde{\mathbf{u}} = Q_{\mathcal{L}}\mathbf{z} \quad \text{with} \quad \mathbf{z}^*G = \tilde{\lambda}\mathbf{z}^*.$$

Since $Q_{\mathcal{L}}^*Q = I_k$ and $\|Q\mathbf{w}\|_2 = 1$ because Q is unitary (i.e., its columns form an orthonormal basis of the search subspace), we have

$$(4.7) \quad \tilde{\delta} := \tilde{\mathbf{u}}^*\tilde{\mathbf{v}} = \frac{\mathbf{z}^*Q_{\mathcal{L}}^*Q\mathbf{w}}{\|Q_{\mathcal{L}}\mathbf{z}\|_2\|Q\mathbf{w}\|_2} = \frac{\mathbf{z}^*\mathbf{w}}{\|Q_{\mathcal{L}}\mathbf{z}\|_2}.$$

Depending on how the reduced problem is formulated, two main variants are introduced in this paper for pseudo-hermitian problems:

- *Rayleigh–Quotient with hermitian spectral equivalence,* leads to solve a reduced hermitian eigenproblem. This allows the use of stable hermitian eigensolvers

(e.g., HEEVD), and preserves many of the favorable spectral properties of H . In particular, this variant produces a tighter control over perturbation sensitivity and creates a pathway for recovering quadratic convergence under stable conditions. While very unlikely in practice, corner cases of failure may happen with this variant of Rayleigh-Ritz. This motivates the implementation of the next variant based on a non-hermitian Rayleigh-Quotient.

- *Rayleigh-Quotient with no hermitian spectral equivalence*, leads to solve a general non-symmetric eigensolver (e.g., GEEV), that is also ready for eventual cases where SH is indefinite. While being more expensive than solving an hermitian eigenvalue problem by nature, this variant can be used as a back-up in case of failure of the hermitian Rayleigh-Quotient.

The subsequent Section 5 develops rigorous error bounds and convergence criteria for the hermitian Rayleigh-Quotient as well as numerical evidences for the non-hermitian one. We analyze how the convergence order—linear versus quadratic—depends on the interplay between the oblique trial subspaces, the conditioning of the dual basis, and key quantities such as $\tilde{\delta}$, σ_u , and σ_v .

5. Oblique Rayleigh–Ritz: Variants and Convergence. The two variants introduced in previous section—*Rayleigh-Quotient with hermitian spectral equivalence* and *Rayleigh-Quotient with no hermitian spectral equivalence*—both rest on the oblique Rayleigh–Ritz principle. Their performance depends critically on how the dual basis $Q_{\mathcal{L}}$ interacts with the search space Q .

5.1. General considerations on Oblique Rayleigh–Ritz. To assess convergence, we first recall the role of the dual basis and derive bounds for the Ritz values in terms of $\tilde{\delta}$ defined in (4.2) and the error coefficients σ_u, σ_v from (4.3). These bounds will serve as the foundation for analyzing conditions under which the method achieves quadratic convergence.

THEOREM 5.1. *The convergence of a Ritz value $\tilde{\lambda}$ in the oblique variant satisfies*

$$(5.1) \quad |\lambda - \tilde{\lambda}| \leq |\tilde{\delta}|^{-1} \cdot |\bar{\sigma}_u \sigma_v| \cdot \|H - \lambda I\|_2.$$

Proof. Using (4.6) and (4.7) we can write

$$(5.2) \quad \tilde{u}^* H \tilde{v} = \frac{\mathbf{z}^* Q_{\mathcal{L}} H Q \mathbf{w}}{\|Q_{\mathcal{L}} \mathbf{z}\|_2} = \frac{\mathbf{z}^* G \mathbf{w}}{\|Q_{\mathcal{L}} \mathbf{z}\|_2} = \tilde{\lambda} \frac{\mathbf{z}^* \mathbf{w}}{\|Q_{\mathcal{L}} \mathbf{z}\|_2} = \tilde{\lambda} \tilde{\delta},$$

which allows us to express the approximate eigenvalue $\tilde{\lambda} = \tilde{\delta}^{-1} \tilde{u}^* H \tilde{v}$. Plugging in the latter expression in the linear decompositions of (4.3) gives

$$(5.3) \quad \begin{aligned} |\lambda - \tilde{\lambda}| &= |\lambda - \tilde{\delta}^{-1} \tilde{u}^* H \tilde{v}| \\ &= |\lambda - \tilde{\delta}^{-1} [\lambda (\bar{\gamma}_u \gamma_v \mathbf{u}^* \mathbf{v} + \bar{\gamma}_u \sigma_v \mathbf{u}^* \mathbf{e}_v + \bar{\sigma}_u \gamma_v \mathbf{e}_u^* \mathbf{v}) + \bar{\sigma}_u \sigma_v \mathbf{e}_u^* H \mathbf{e}_v]|. \end{aligned}$$

Expanding the scalar product $\tilde{\delta} := \tilde{u}^* \tilde{v}$ with (4.3) leads to

$$(5.4) \quad \tilde{\delta} - \bar{\sigma}_u \sigma_v \mathbf{e}_u^* \mathbf{e}_v = \bar{\gamma}_u \gamma_v \mathbf{u}^* \mathbf{v} + \bar{\gamma}_u \sigma_v \mathbf{u}^* \mathbf{e}_v + \bar{\sigma}_u \gamma_v \mathbf{e}_u^* \mathbf{v}.$$

Plugging (5.4) back into (5.3) results in

$$(5.5) \quad \begin{aligned} |\lambda - \tilde{\lambda}| &= |\lambda - \tilde{\delta}^{-1} [\lambda (\tilde{\delta} - \bar{\sigma}_u \sigma_v \mathbf{e}_u^* \mathbf{e}_v) - \bar{\sigma}_u \sigma_v \mathbf{e}_u^* H \mathbf{e}_v]| \\ &= |\tilde{\delta}|^{-1} \cdot |\bar{\sigma}_u \sigma_v \mathbf{e}_u^* (H - \lambda I) \mathbf{e}_v|, \end{aligned}$$

which provides an upper bound on the error and proves the statement of the theorem

$$(5.6) \quad |\lambda - \tilde{\lambda}| \leq |\tilde{\delta}|^{-1} \cdot |\bar{\sigma}_u \sigma_v| \cdot \|H - \lambda I\|_2. \quad \square$$

Remark 5.2 (hermitian case). If H is hermitian, then left and right eigenvectors coincide: $\mathbf{u} = \mathbf{v}$. Consequently, $\tilde{\delta} = 1$ and $|\bar{\sigma}_u \sigma_v| = |\sigma_v|^2$. Hence, the bound reduces to

$$|\lambda - \tilde{\lambda}| \leq |\sigma_v|^2 \|H - \lambda I\|_2,$$

recovering the classical quadratic convergence of the hermitian Rayleigh–Ritz of (2.2).

Remark 5.3 (Non-hermitian case). For non-hermitian or pseudo-hermitian H , left and right eigenvectors generally differ. Then $|\tilde{\delta}| < 1$ and $|\sigma_u|$ may differ from $|\sigma_v|$. Two key factors control convergence:

1. *Subspace projection errors*: The quantities σ_u and σ_v measure the misalignment of the search subspaces with the left and right invariant subspaces. Quadratic convergence occurs only if $|\sigma_u|$ and $|\sigma_v|$ are of the same order of magnitude.
2. *Dual subspace alignment*: The factor $|\tilde{\delta}|^{-1}$ amplifies the error if the approximate left and right subspaces are poorly aligned. Convergence is more predictable if $|\tilde{\delta}|^{-1}$ can be bounded by a constant independent of σ_u , σ_v , and $\tilde{\lambda}$.

Unlike the hermitian case, the error in non-hermitian Rayleigh–Ritz depends both on how well the right eigenvectors are captured and how accurately the dual (left) subspace is approximated. The oblique procedure mitigates cross-term contamination by constructing a dual basis, but convergence is no longer automatically quadratic. Proper alignment of both subspace and control of $|\tilde{\delta}|$ are essential for fast convergence. Regarding the first point on the order of magnitude of σ_v and σ_u , we first note that

$$(5.7) \quad |\sigma_v| \geq \|(I - \Pi(Q))\mathbf{v}\|_2 \quad \text{and} \quad |\sigma_u| \geq \|(I - \Pi(Q_{\mathcal{L}}))\mathbf{u}\|_2,$$

where $\Pi(Q) := Q(Q^*Q)^{-1}Q^*$ denotes the ℓ_2 -orthogonal projection onto $\text{range}(Q)$ (similarly for $\Pi(Q_{\mathcal{L}})$); see, e.g., [20, section 4.3.1]. In other words, σ_v (resp., σ_u) measures the component of the exact eigenvector \mathbf{v} (resp., \mathbf{u}) that lies outside the subspace spanned by Q (resp., $Q_{\mathcal{L}}$). These inequalities highlight that convergence depends critically on the alignment of the subspace Q and $Q_{\mathcal{L}}$ with the true right and left invariant subspaces. Importantly, even if Q approximates \mathbf{v} well, there is no guarantee that $Q_{\mathcal{L}}$ approximates \mathbf{u} equally well. When the magnitudes of $|\sigma_u|$ and $|\sigma_v|$ differ significantly, the product $|\sigma_u \sigma_v|$ in the error bound becomes dominated by the larger term, leading to only linear rather than quadratic convergence.

Ideally, we seek a dual basis $Q_{\mathcal{L}}$ such that the components of \mathbf{u} and \mathbf{v} outside their respective subspaces are of similar magnitude, i.e.,

$$(5.8) \quad \|(I - \Pi(Q_{\mathcal{L}}))\mathbf{u}\|_2 = \|(I - \Pi(Q))\mathbf{v}\|_2,$$

ensuring that the convergence of the Ritz values is as fast as possible.

For the second point on identifying a constant upper bound for $|\tilde{\delta}|^{-1}$, the following theorem relates it to the norm of the dual basis $Q_{\mathcal{L}}$ and the eigenvalue condition

number of the Rayleigh-Quotient G . In what follows, we indicate the eigenvalue condition number of the Rayleigh-Quotient G with $\text{cond}(\tilde{\lambda}, G) := (|\mathbf{z}^* \mathbf{w}|)^{-1}$, where \mathbf{z} and \mathbf{w} are respectively a left and right eigenvector as defined in (4.6). Similarly to the usual interpretation of the condition number of a matrix, the eigenvalue condition number relates the perturbation on an eigenvalue with a perturbation on the matrix: when $\text{cond}(\tilde{\lambda}, G)$ is large, a small perturbation on G can produce a large perturbation of $\tilde{\lambda}$. This quantity therefore provides an indication on the numerical stability of the eigensolver (see [26, chapter 2]).

LEMMA 5.4. *Let $\text{cond}(\tilde{\lambda}, G)$ be an eigenvalue condition number of the Rayleigh-Quotient G given in (4.5). Then, the oblique overlap $|\tilde{\delta}|^{-1}$ is bounded as follows*

$$(5.9) \quad |\tilde{\delta}|^{-1} \leq \text{cond}(\tilde{\lambda}, G) \cdot \|Q_{\mathcal{L}}\|_2.$$

Proof. The proof is a direct consequence of (4.7). The eigenvalue condition number being defined as the inverse of the angle between the associated left and right eigenvectors such that $\text{cond}(\tilde{\lambda}, G) := (|\mathbf{z}^* \mathbf{w}|)^{-1}$, we simply have

$$(5.10) \quad |\tilde{\delta}| = \frac{|\mathbf{z}^* \mathbf{w}|}{\|Q_{\mathcal{L}} \mathbf{z}\|_2} = \frac{\text{cond}(\tilde{\lambda}, G)^{-1}}{\|Q_{\mathcal{L}} \mathbf{z}\|_2} \Rightarrow |\tilde{\delta}|^{-1} \leq \text{cond}(\tilde{\lambda}, G) \cdot \|Q_{\mathcal{L}}\|_2. \quad \square$$

In the perspective of decreasing the upper bound of $|\tilde{\delta}|^{-1}$ in (5.9), one could in principle simply set $Q_{\mathcal{L}} := Q$, because $Q^* Q = I_k$. However, this choice does not control $\text{cond}(\tilde{\lambda}, G)$: the reduced problem may still be ill-conditioned, and $\text{cond}(\tilde{\lambda}, G)$ can dominate the bound. Thus $Q_{\mathcal{L}} = Q$ is not a panacea. Especially, we have

$$\begin{aligned} \|(I - \Pi(Q)) \mathbf{u}\|_2 &= \|(S - Q Q^* S) \mathbf{v}\|_2 \\ &= \|(I - \Pi(Q)) \mathbf{v} + 2X\mathbf{v}\|_2 \quad \text{with} \quad X := \begin{bmatrix} 0 & Q_1 Q_2^* \\ 0 & Q_2 Q_2^* - I \end{bmatrix}, \end{aligned}$$

where Q_1 and Q_2 respectively stand for the upper and lower part of Q , such that

$$(5.11) \quad Q = \begin{bmatrix} Q_1 \\ Q_2 \end{bmatrix}.$$

This extra $2X\mathbf{v}$ stems from the pseudo-hermitian sign-flip relation between left and right eigenvectors and can be non-negligible, so even a small right-project error does not guarantee a small left-projection error. This explains why $|\sigma_{\mathbf{v}}|$ and $|\sigma_{\mathbf{u}}|$ can differ substantially and motivates designing $Q_{\mathcal{L}}$ so that it directly approximates the left invariant subspace rather than relying on $Q_{\mathcal{L}} = Q$.

The dual basis $Q_{\mathcal{L}}$ should satisfy a trade-off between the four following criteria, introduced in descending order of importance.

1. *Biorthogonality with Q .* The essential condition is that $Q_{\mathcal{L}}^* Q = I_k$. Without this biorthogonality, the Rayleigh-Ritz method would no longer act as a projection (see (4.4)), and the whole framework would break down.
2. *Computational feasibility.* Constructing G must remain practical and not introduce a computational bottleneck.
3. *Representation of left eigenvectors.* The range of $Q_{\mathcal{L}}$ should enable a correct representation of the target left eigenvectors. Ideally, the ℓ_2 -projection operators $\Pi(Q_{\mathcal{L}})$ and $\Pi(Q)$ yield the same lower bounds in (5.7) when applied

respectively to left and right eigenvectors, so that the the equality (5.8) holds. In this case, it is natural to expect that the stability parameters σ_u and σ_v have the same order of magnitude (i.e., $\mathcal{O}(\sigma_u) = \mathcal{O}(\sigma_v)$).

4. *Small constant upper bound for $|\tilde{\delta}|^{-1}$.* Provided the previous condition holds, one further requires that $|\tilde{\delta}|^{-1}$ admit an upper bound independent of σ_v , σ_u and $\tilde{\lambda}$. This ensures that Ritz values converge quadratically with respect to σ_v , mirroring the hermitian case. Thus, the fourth criterion is that Q_L should provide such a bounded constant, enabling the non-hermitian Rayleigh–Ritz procedure to achieve the same quadratic convergence rate as in the hermitian theory.

Before introducing practical implementations, we present a general form of dual basis that always satisfies the orthonormality requirement with Q .

DEFINITION 5.5. *Let M be a non-singular matrix. A dual basis Q_L is defined as*

$$(5.12) \quad Q_L := [SQ - Q(Q^*SQ - M)]M^{-1}.$$

Since Q is orthonormal ($Q^*Q = I_k$), we have

$$(5.13) \quad \begin{aligned} Q_L^*Q &= \left([SQ - Q(Q^*SQ - M)]M^{-1} \right)^* Q \\ &= (M^{-1})^*(Q^*S^* - (Q^*SQ - M)^*Q^*)Q \\ &= (M^{-1})^*(Q^*S^*Q - Q^*S^*Q + M^*) \\ &= (M^{-1})^*M^* \\ &= I. \end{aligned}$$

Thus, Q_L is indeed biorthogonal to Q , satisfying $Q_L^*Q = I_k$. The form of Q_L in Definition 5.5 is designed to mimic the relation $U = SV$ for pseudo-hermitian Hamiltonians (3.5). The key difference is that we subtract from SQ the subspace component already contained in the range of Q . The matrix M determines the amount that is subtracted. Eliminating the entire subspace would not work since Q_L and Q must overlap to satisfy the condition $Q_L^*Q = I_k$. Setting $M = 0$ would, for instance, achieve full subtraction, which is equivalent to set $Q_L^*Q = 0$, but this is avoided by requiring M to be non-singular. All dual bases introduced subsequently adhere to the form (5.12), which guarantees the first criterion—orthonormality of Q_L with Q —as long as M remains non-singular. Regarding the second criterion on *Computational feasibility*, point of performance and scalability, the next section introduces a specific choice of M that reduces the problem to a hermitian eigenvalue problem.

5.2. Rayleigh-Quotient with hermitian spectral equivalence. In this section, we show that by choosing

$$(5.14) \quad M := Q^*SQ,$$

it leads to an oblique Rayleigh–Ritz which solves an hermitian eigenvalue problem. The corresponding dual space is

$$(5.15) \quad Q_L := SQ(Q^*SQ)^{-1}.$$

By construction, $Q_L^*Q = I_k$, ensuring that the bi-orthogonality property required for Rayleigh–Ritz is satisfied. The associated Rayleigh-Quotient (4.5) then reads

$$(5.16) \quad G = (Q^*SQ)^{-1}Q^*SHQ.$$

Notice that both Q^*SQ and Q^*SHQ in (5.16) are hermitian. Furthermore, if the pseudo-hermitian condition (1.4) holds, then Q^*SHQ is positive definite.

For the development that follows, we assume that $M = Q^*SQ$ is non-singular and discuss its eventual singularity thereafter. In general, solving $G\mathbf{w} = \tilde{\lambda}\mathbf{w}$ would require a non-hermitian eigensolver, as G is generally non-hermitian. However, we can exploit the positive-definiteness of SH to solve an equivalent hermitian eigenvalue problem.

THEOREM 5.6. *Let $Q^*SHQ = LL^*$ be the Cholesky factorization, with L the lower triangular factor. Then, the Ritz values $\tilde{\lambda}$ and the corresponding right and left Ritz vectors \mathbf{z} and \mathbf{w} satisfy*

$$(5.17) \quad L^*(Q^*SQ)^{-1}Ly = \tilde{\lambda}y, \quad \text{with} \quad \mathbf{y} = L^*\mathbf{w} \quad \text{and} \quad \mathbf{z} = Ly.$$

Proof. Define $\mathbf{y} = L^*\mathbf{w}$. Then, we have

$$(5.18) \quad G\mathbf{w} = (Q^*SQ)^{-1}Q^*SHQ\mathbf{w} = \tilde{\lambda}\mathbf{w} \quad \Leftrightarrow \quad (Q^*SQ)^{-1}Ly = \tilde{\lambda}L^{-*}\mathbf{y}.$$

Left multiplying by L^* leads to the hermitian eigenvalue problem (5.17), which defines \mathbf{y} . Similarly, by taking the transpose-conjugate and multiplying from the right with L^{-*} the left Ritz vector is $\mathbf{z} = Ly$, and its eigenvalues $\tilde{\lambda}$ are guaranteed to be real. \square

This equivalence has several important consequences.

1. *Hermitian solver:* The spectral reduction to the hermitian problem (5.17) allows the use of specialized hermitian eigensolvers such as **HEEVD**, which are faster and more stable than general eigensolvers like **GEEV**. The only additional cost is the Cholesky factorization of the Q^*SHQ matrix, which has size $k \times k$.
2. *Efficient inversion:* The explicit inversion of Q^*SQ can be avoided by formulating the inverse eigenproblem. In practice, one constructs the inverted Rayleigh-Quotient by applying backward substitution with L^* on the right, followed by forward substitution with L on the left (see Line 7 in Algorithm 2.1).
3. *Reality of Ritz values:* Because the transformed problem is hermitian, all Ritz values are real, in agreement with the spectral properties of H described in Section 3.2.

The hermitian spectrally equivalent Rayleigh-Quotient is built without explicit construction of the dual space $Q_{\mathcal{L}}$. The Rayleigh-Ritz method is summarized in Algorithm 5.1, where the right comments contain the name of the CPU kernels along with an estimation of their computational complexity. Since the index k represents the number of columns of Q , it initially corresponds to **nevex** but decreases with the number of converged locked eigenvectors (i.e., $k = \text{nevex} - \text{locked}$). Clearly, the computational cost is dominated by the first **GEMM** operation at line one since $k \ll n$. We now turn to the third and fourth conditions required for quadratic convergence. The following theorem establishes that the ideal relation in (5.8) holds in with the setting above.

THEOREM 5.7. *Let $Q_{\mathcal{L}}$ be defined as in (5.25), namely $Q_{\mathcal{L}} = SQ(Q^*SQ)^{-1}$. Then, the ℓ_2 -orthogonal projection operators $\Pi(Q)$ and $\Pi(Q_{\mathcal{L}})$ satisfy*

$$(5.19) \quad \|(I - \Pi(Q_{\mathcal{L}}))\mathbf{u}\|_2 = \|(I - \Pi(Q))\mathbf{v}\|_2.$$

Proof. Developing the ℓ_2 -projection $\Pi(Q_{\mathcal{L}})$ gives

$$(5.20) \quad \begin{aligned} \Pi(Q_{\mathcal{L}}) &= Q_{\mathcal{L}}(Q_{\mathcal{L}}^*Q_{\mathcal{L}})^{-1}Q_{\mathcal{L}}^* \\ &= SQ(Q^*SQ)^{-1}(Q^*SQ)^2(Q^*SQ)^{-1}Q^*S = SQQ^*S. \end{aligned}$$

Algorithm 5.1 Sequential construction of the hermitian Rayleigh Quotient

-
- | | |
|---|---------------------------------|
| 1: Compute $T \leftarrow HQ$ | ▷ BLAS GEMM $n^2 k$ |
| 2: Flip the sign of the lower half $T \leftarrow ST$ | ▷ INTERNAL FLIP $\frac{n}{2} k$ |
| 3: Compute $W \leftarrow Q^*T$ | ▷ BLAS GEMM nk^2 |
| 4: Factorize $L \leftarrow \text{CHOLESKY}(W)$ | ▷ LLAPACK PORTF k^3 |
| 5: Compute $M \leftarrow I - 2Q_2^*Q_2$ ($= Q^*SQ$) | ▷ BLAS GEMM $\frac{n^2}{4} k$ |
| 6: Copy $G \leftarrow M$ | ▷ BLAS COPY k^2 |
| 7: Solve $G \leftarrow L^{-1}(GL^{-*})$ | ▷ 2 LLAPACK TRSM $2k^2$ |
| 8: Solve $GY = \tilde{\Lambda}Y$ | ▷ LLAPACK HEEVD k^3 |
| 9: Back-transform $\tilde{\Lambda}, Y \leftarrow \tilde{\Lambda}^{-1}, L^{-1}Y$ | ▷ LLAPACK TRSM k^2 |
| 10: Return $\tilde{\Lambda}, Y$ | |
-

Next, recall that $\mathbf{u} = S\mathbf{v}$. Since Q has orthonormal columns, we obtain

$$(5.21) \quad (I - \Pi(Q_{\mathcal{L}}))\mathbf{u} = S\mathbf{v} - SQQ^*\mathbf{v} = S(I - \Pi(Q))\mathbf{v}.$$

Finally, because S is unitary, it preserves the ℓ_2 -norm. Hence

$$(5.22) \quad \|(I - \Pi(Q_{\mathcal{L}}))\mathbf{u}\|_2 = \|S(I - \Pi(Q))\mathbf{v}\|_2 = \|(I - \Pi(Q))\mathbf{v}\|_2,$$

proving (5.19). □

From this result, we conclude that $Q_{\mathcal{L}}$ and Q approximate \mathbf{u} and \mathbf{v} with identical accuracy. Consequently, $\mathcal{O}(\sigma_{\mathbf{u}}) \approx \mathcal{O}(\sigma_{\mathbf{v}})$, which implies $|\bar{\sigma}_{\mathbf{u}}\sigma_{\mathbf{v}}| = \mathcal{O}(\sigma_{\mathbf{v}}^2)$.

For what follows, let $\lambda_{\min}(\cdot)$ and $\lambda_{\max}(\cdot)$ respectively be the minimum and maximum eigenvalue in magnitude of the designated matrix between parenthesis. To complete the proof of quadratic convergence of the Ritz values, it remains to establish an upper bound for $|\tilde{\delta}|^{-1}$ that is independent of both $\sigma_{\mathbf{v}}$ and of the Ritz value $\tilde{\lambda}$. This bound is derived in the next theorem, which refines Theorem 5.4.

THEOREM 5.8. *The parameter $|\tilde{\delta}|^{-1}$ is bounded as follows*

$$(5.23) \quad |\tilde{\delta}|^{-1} \leq \frac{\sqrt{\text{cond}(H)}}{|\lambda_{\min}(Q^*SQ)|}.$$

Proof. By Theorem 5.4, we need to control $\|Q_{\mathcal{L}}\|_2$ and the eigenvalue condition number $\text{cond}(\tilde{\lambda}, G)$. First, recall that

$$(5.24) \quad \|Q_{\mathcal{L}}\|_2^2 = \sigma_{\max}(Q_{\mathcal{L}})^2 = \lambda_{\max}(Q_{\mathcal{L}}^*Q_{\mathcal{L}}).$$

For the general form (5.12), one obtains

$$(5.25) \quad \begin{aligned} Q_{\mathcal{L}}^*Q_{\mathcal{L}} &= (M^{-1})^* \left[Q^*SSQ - 2(Q^*SQ)^2 + Q^*Q \cdot (Q^*SQ)^2 \right] M^{-1} + Q^*Q \\ &= (M^{-1})^* \left[I - (Q^*SQ)^2 \right] M^{-1} + I, \end{aligned}$$

which gives the following ℓ_2 -norm

$$(5.26) \quad \|Q_{\mathcal{L}}\|_2^2 = 1 + \lambda_{\max} \left((M^{-1})^* \left[I - (Q^*SQ)^2 \right] M^{-1} \right).$$

With $M = Q^*SQ$, this reduces to

$$(5.27) \quad \|Q_L\|_2 = \left(\sqrt{\lambda_{\min}(Q^*SQ)^2} \right)^{-1} = \frac{1}{|\lambda_{\min}(Q^*SQ)|}.$$

Second, the eigenvalue condition number of G is given by the inverse of the angle between the normalized left and right eigenvectors. Recall that $Q^*SHQ = LL^*$ is the Cholesky factorization, then, for a normalized eigenvector \mathbf{y} of the reduced hermitian matrix (5.17), we have

$$(5.28) \quad \text{cond}(\tilde{\lambda}, G) = \frac{\|\mathbf{w}\|_2 \|\mathbf{z}\|_2}{|\mathbf{w}^* \mathbf{z}|} = \frac{\|\mathbf{y}^* L^{-1}\|_2 \|L\mathbf{y}\|_2}{|\mathbf{y}^* L^{-1} L \mathbf{y}|} \leq \sqrt{\text{cond}(Q^*SHQ)}.$$

Since SH is hermitian (see (1.4)) and Q is unitary, the eigenvalues of Q^*SHQ interlace those of SH . Therefore

$$(5.29) \quad \text{cond}(\tilde{\lambda}, G) \leq \sqrt{\text{cond}(SH)} = \sqrt{\text{cond}(H)},$$

where the last equality follows from Theorem 3.5. Combining both estimates gives

$$(5.30) \quad |\tilde{\delta}|^{-1} \leq \frac{\sqrt{\text{cond}(H)}}{|\lambda_{\min}(Q^*SQ)|}. \quad \square$$

The denominator $|\lambda_{\min}(Q^*SQ)|$ does not depend on σ_v or on the target Ritz value $\tilde{\lambda}$. While this quantity may approach zero in degenerate cases, in practice it is typically well-conditioned (see below for a further discussion).

To summarize, both the third and fourth criteria for quadratic convergence are satisfied. Since $\mathcal{O}(\sigma_u) = \mathcal{O}(\sigma_v)$ and $|\tilde{\delta}|^{-1}$ is bounded independently of σ_v and $\tilde{\lambda}$, the Ritz values converge quadratically. This is stipulated by the next lemma.

LEMMA 5.9. *The Ritz values converge quadratically, in the sense that*

$$(5.31) \quad |\lambda - \tilde{\lambda}| \leq \kappa \cdot \mathcal{O}(\sigma_v^2) \quad \text{with} \quad \kappa := \frac{\sqrt{\text{cond}(H)} \cdot \|H - \lambda I\|_2}{|\lambda_{\min}(Q^*SQ)|}.$$

The quadratic convergence of the Ritz-values is thus established. The bound depends primarily on the condition number of H and the smallest eigenvalue in magnitude of Q^*SQ . Although this framework provides strong guarantees in terms of performance and convergence, difficulties arise when $\lambda_{\min}(Q^*SQ)$ is very close to zero, since in that case the denominator may drastically amplify the bound. Such situations are rare in practice but cannot be ruled out *a priori*. Because S has the structure (1.2) and Q is unitary, Cauchy's interlacing theorem ensures that the spectrum of Q^*SQ is contained in the interval $[-1, 1]$. Consequently, the denominator always acts to enlarge the upper bound κ . The next theorem sharpens this observation by providing an explicit interval in which the Ritz values must lie, showing how $\lambda_{\min}(Q^*SQ)$ effectively stretches that interval.

THEOREM 5.10. *Assume Q^*SQ is non-singular. Then the Ritz values are all located within a closed interval, namely*

$$(5.32) \quad \tilde{\lambda} \in \left[-\frac{\rho(SH)}{|\lambda_{\min}(Q^*SQ)|}, \frac{\rho(SH)}{|\lambda_{\min}(Q^*SQ)|} \right].$$

Proof. See the proof in Appendix B. \square

This result complements Theorem 5.9: while the bound κ already reveals how a small eigenvalue of Q^*SQ can deteriorate convergence, Theorem 5.10 shows that it also enlarges the admissible interval in which the Ritz values may lie. In particular, since A is a principal submatrix of SH and that Lemma 3.4 established that the true eigenvalues are located within $[-\rho(A), \rho(A)]$, we have

$$\lambda \in [-\rho(A), \rho(A)] \subseteq [-\rho(SH), \rho(SH)] \subseteq \left[-\frac{\rho(SH)}{|\lambda_{\min}(Q^*SQ)|}, \frac{\rho(SH)}{|\lambda_{\min}(Q^*SQ)|} \right].$$

Any Ritz-values falling outside this interval can therefore be regarded as “spurious values”. And the domain where such spurious values appear expands as $\lambda_{\min}(Q^*SQ)$ decreases. These observations show the importance of addressing the possible near-singularity—or worse, rank deficiency—of Q^*SQ . At this stage, nothing prevents $\lambda_{\min}(Q^*SQ)$ from being arbitrarily close to zero. A more refined understanding is obtained by decomposing Q into its upper and lower blocks Q_1 and Q_2 , as in (5.11), and relating the spectrum of (Q^*SQ) to the singular values $\sigma_i(Q_1)$, with $\sigma_i(Q_1)$ the i th largest singular value of Q_1 . The next theorem makes this connection explicit and clarifies under which circumstances a small eigenvalue of Q^*SQ can occur.

THEOREM 5.11. *The eigenvalues of Q^*SQ are given by*

$$(5.33) \quad \lambda_i(Q^*SQ) = 2\sigma_i^2(Q_1) - 1 \quad , \quad \forall i = 1, \dots, \text{nevex}$$

Proof. Recall that $Q^*Q = I$. Therefore, we have $Q^*SQ = Q_1^*Q_1 - Q_2^*Q_2 = 2Q_1^*Q_1 - I$. Let the singular value decomposition of Q_1 be $Q_1 = U_1\Sigma_1V_1^*$. Then, we also have $Q_1^*Q_1 = V_1\Sigma_1^2V_1^*$, which implies that $Q^*SQ = V_1(2\Sigma_1^2 - I)V_1^*$. Therefore the eigenvalues of Q^*SQ are

$$(5.34) \quad \lambda_i(Q^*SQ) = 2\lambda_i(Q_1^*Q_1) - 1 = 2[\Sigma_1^2]_{i,i} - 1 = 2\sigma_i^2(Q_1) - 1. \quad \square$$

Remark 5.12. From $Q^*Q = I$ it follows that $Q_2^*Q_2 = I - Q_1^*Q_1 = V_1(I - \Sigma_1^2)V_1^*$. Hence Q_1 and Q_2 share the same right singular vectors, and their singular values are related by $\sigma_i(Q_2)^2 = 1 - \sigma_i(Q_1)^2$.

Theorem 5.11 highlights that the near-singularity of Q^*SQ is not governed by σ_v but rather by the interplay between Q_1 and Q_2 . For example, enforcing $Q_2 = 0$ would ensure

$$Q_2 := 0 \quad \Rightarrow \quad \lambda_{\min}(Q^*SQ) = 1 \quad \Leftrightarrow \quad \kappa = \sqrt{\text{cond}(H)} \cdot \|H - \lambda I\|_2,$$

thus reducing the upper bound κ in Lemma 5.9. However, this comes at the expense of destroying the range of Q , which increases the coefficient σ_v due to (5.7). Conversely, a large σ_v does not necessarily imply a small $\lambda_{\min}(Q^*SQ)$. The worst case scenario occurs when $\sigma_i(Q_1) = \sigma_i(Q_2) = 1/\sqrt{2}$ holds. In this situation, a component of the range of Q_1 and a component of the range of Q_2 contribute equally to the span of Q . Their contributions cancel in Q^*SQ , since

$$(5.35) \quad Q^*SQ = V_1[\Sigma_1^2 - (I - \Sigma_1^2)]V_1^*,$$

which makes the matrix singular. When this happens, the eigenvalue problem (5.17) cannot be solved. Importantly, this degeneracy is not a matter of numerical instability; it is inherent to the structure of the dual basis $Q_{\mathcal{L}}$. Indeed, the relationship

between Q and Q_L replicates that between U and V . From U and V to form a bi-orthogonal system such that $U^*V = V^*SV = D$ (see (3.10)), the diagonal matrix D must be non-singular. Accordingly, Q^*SQ must also be non-singular.

In summary, the possible singularity of Q^*SQ is not a numerical artifact but a structural property of the problem itself. While this corner case rarely arise in practice, it warrants careful consideration. To safeguard against this eventuality, the next section introduces an alternative construction based on a matrix M that defines the dual basis Q_L (5.12) without requiring the inversion of Q^*SQ . This alternative serves as a fallback strategy, while the setting $M := Q^*SQ$ as the “default” approach.

5.3. Non-hermitian Rayleigh-Quotient as back-up. This framework will only be used in the corner cases of failure of the default hermitian eigenproblem where Q^*SQ turns out to be singular. Here, we want to ensure that the alternative M matrix is always non-singular and well-conditioned. One straightforward and practical choice that is very easy to check is setting $M := \text{diag}(Q^*SQ)$. In that case, the dual basis becomes

$$(5.36) \quad Q_L := [SQ - Q(Q^*SQ - \text{diag}(Q^*SQ))] \text{diag}^{-1}(Q^*SQ),$$

and the Rayleigh-Quotient G is given by

$$(5.37) \quad G = \text{diag}^{-1}(Q^*SQ) [Q^*SHQ - (Q^*SQ - \text{diag}(Q^*SQ)) Q^*HQ].$$

As expected, this matrix G is not hermitian, and has no hermitian spectral equivalence due to the appearance of Q^*HQ in (5.37). Hence, the Ritz-values are all complex. Therefore, we keep only the real parts in practice. In addition, the ideal equality (5.19) does not apply here. Therefore, the approximation error of the eigenvalues is unlikely to decrease quadratically with respect to σ_v , which motivates resorting to this implementation only as a back-up option in case of failure of the default setting $M := Q^*SQ$. In the eventual case where a zero entries appear in $\text{diag}(Q^*SQ)$, one can always replace it with 1s without breaking the projection properties of Rayleigh-Ritz. The practical implementation of this non-hermitian Rayleigh-Ritz variant is summarized in Algorithm 5.2.

Algorithm 5.2 Sequential construction of the non-hermitian Rayleigh Quotient

- 1: Compute $T \leftarrow HQ$ ▷ BLAS GEMM n^2k
 - 2: Compute $W \leftarrow Q^*T$ ▷ BLAS GEMM nk^2
 - 3: Compute $M \leftarrow -2Q_2^*Q_2$ ▷ BLAS GEMM $\frac{n^2}{4}k$
 - 4: Compute the diagonal $\mathbf{d} \leftarrow (1 + \text{diag}(M))^{-1}$ ▷ BLAS ADD k
 - 5: Compute $M \leftarrow M - \text{diag}(M)$ ($= Q^*SQ - \text{diag}(Q^*SQ)$) ▷ BLAS ADD k
 - 6: Flip the sign of the lower half $T \leftarrow ST$ ▷ INTERNAL FLIP $\frac{n}{2}k$
 - 7: Compute $G \leftarrow Q^*T$ ▷ BLAS GEMM nk^2
 - 8: Compute $G \leftarrow MW + G$ ▷ BLAS GEMM k^3
 - 9: Scale $G \leftarrow \text{Diag}(\mathbf{d}) \cdot G$ ▷ BLAS SCAL k^2
 - 10: Solve $GY = \tilde{\Lambda}Y$ ▷ LAPACK GEEV k^3
 - 11: Return $\tilde{\Lambda}, Y$
-

Figure 5.1 and Figure 5.2 show the evolution of the residual errors $\|H\tilde{\mathbf{v}}_i - \tilde{\lambda}_i\tilde{\mathbf{v}}_i\|_2$ with respect to the number of iterations for two real world matrices generated from

Yambo [15]. Green curves show the convergence with the *hermitian spectrally equivalent Rayleigh-Quotient* (HEEVD) and blue curves depict the convergence when using the alternative *non-hermitian Rayleigh-Quotient* (GEEV). The red lines represent the evolution of the residuals in the standard version of ChASE when applied to a spectrally equivalent hermitian matrix generated artificially. For the first hundred smallest eigenpairs appearing in Figure 5.1a, the rates of convergence for the three different implementations appear very similar. However, the GEEV implementation stagnates around a slightly higher residual error than the two other variants. On the other hand, the second subfigure 5.1b focusing on the last eigenpairs ranging from index 900 to index 1000 reveals a clear difference between the standard version of ChASE and the pseudo-hermitian ones. While the standard implementation starts stagnating below 10^{-13} after the 4th iteration, the pseudo-hermitian implementations require two to three more iterations to reach the same residual error. That said in practice, the parameter μ_{nevex} is updated at each iteration to track only the remaining portion of non-converged eigenpairs. These observations hold for the larger test case illustrated in Figure 5.2.

While describing the convergence properties for each eigenpair is quite complex, the experiments show that the *non-hermitian Rayleigh-Ritz* approach can be a viable component for expanding ChASE to solve for certain pseudo-hermitian Hamiltonians. This is confirmed in the further convergence experiments illustrated in Figure 7.1. The HEEVD variant demonstrates a faster convergence while offering a cheaper numerical complexity and smaller memory requirement. That said, GEEV remains a suitable choice in certain cases. Moreover, we recall that the latter approach does not rely on the positive-definiteness assumption of SH as stated in (1.4). Hence, this implementation may be a good candidate in expanding ChASE functionalities to the more general case where SH is indefinite.

6. Parallel Implementation of ChASE. We now turn to practical aspects of the parallel implementation of ChASE expansion to pseudo-hermitian problems. ChASE employs a hybrid parallelization strategy tailored to efficiently handle large-scale eigenproblems on distributed-memory systems. The Chebyshev filter is applied on a 2D MPI process grid, with the number of processes chosen to form a nearly square layout whenever possible, which is preferred to balance communication and computation. The Hamiltonian matrix is distributed in a 2D block-block or block-cyclic fashion over 2D MPI grid, while the search subspace, represented as a rectangular matrix, is distributed within one-dimensional row or column communicators, depending on the polynomial degree of the filter. The filtering step may therefore involve collective allreduce operations along either the row or column communicators of the 2D grid. In the implementation of ChASE, the polynomial degree is restricted to be even, ensuring that the filtered vectors remain consistently distributed within the column communicators.

The QR factorization (Algorithm 2.1 Line 5), Rayleigh-Ritz procedure (Algorithm 2.1 Lines 7-9) and the residual computation (Algorithm 2.1 Line 10) kernels, which involve the search subspace, in contrast, are performed on one-dimensional sub-communicators derived from the underlying 2D MPI process grid. Depending on the kernel, either column or row communicators are employed. Within each sub-communicator, these kernels are executed in parallel, while the resulting QR factors, Ritz pairs and residuals are replicated across all corresponding sub-communicators.

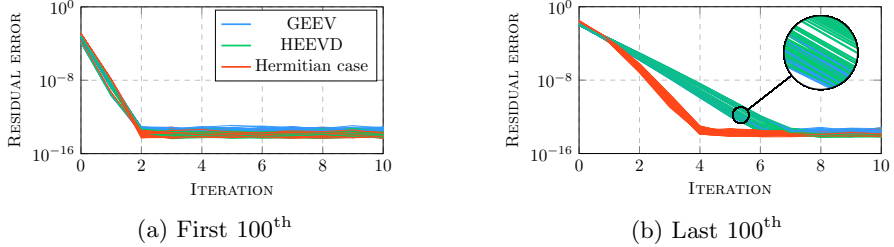


Fig. 5.1: Evolution of the first 100th vs. last 100th residuals out of $\text{nev} = 1000$ smallest eigenpairs for a Silicon pseudo-hermitian Hamiltonian of size $n = 23552$ generated with Yambo

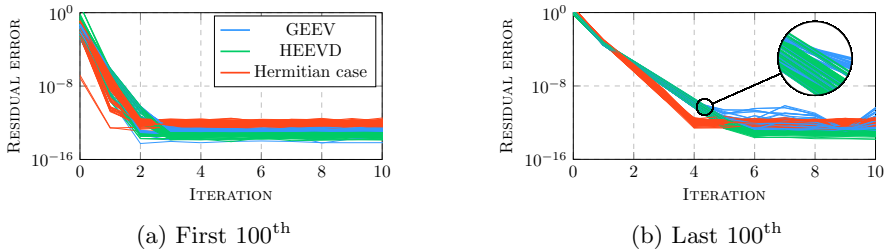


Fig. 5.2: Evolution of the first 100th vs. last 100th residuals out of $\text{nev} = 645$ smallest eigenpairs for a Molybdenum Disulfide pseudo-hermitian Hamiltonian of size $n = 64512$ generated with Yambo

In particular, the solution of the reduced eigenproblem (Algorithm 2.1 Line 8) is performed redundantly on all MPI ranks.

Such a separation of parallelism—2D for filtering and 1D for QR, Rayleigh-Ritz and residual kernels—ensures that all the computation kernels achieve high efficiency. This design also naturally accommodates the optimized filter profile based on the matrix structure. For distributed-GPU architectures, ChASE assigns one GPU per MPI rank and employs the NVIDIA Collective Communications Library (NCCL) for efficient collective operations across devices. All BLAS/LAPACK kernels are executed via the corresponding cuBLAS and cuSOLVER GPU implementations. For further details on the parallel design and implementation choices, we refer the reader to [29].

The filtering of the search space relies on a sequence of **GEMM** operations. When the search space is distributed within each column communicator of the 2D MPI grid, a straightforward parallel **GEMM** would require communicating the row blocks of the matrix to the processes associated with the same column index. In the current implementation of ChASE for hermitian problems, this communication overhead is avoided by leveraging the hermitian structure of the matrix, allowing each process to operate solely on its local data prior to a final reduction step. More precisely, the multiplication of each row of A with the search subspace Q is emulated by multiplying the transpose conjugate of the corresponding column blocks.

In the pseudo-hermitian setting, this approach cannot be applied directly. However,

the defining relation (1.2), namely $H = SH^*S$, yields the equivalence

$$(6.1) \quad H\hat{V} = W \quad \Leftrightarrow \quad H^*S\hat{V} = SW.$$

This identity enables a communication-avoiding formulation of the filtering step in the pseudo-hermitian case. Specifically, the sign pattern encoded in S is applied to the input search space \hat{V} prior to the matrix product, after which the conjugate transpose H^* is multiplied locally. The desired result W is then recovered by re-multiplying S to the intermediate output, since $W = S(SW)$. In practice, all sign-flip operations corresponding to implicit multiplication by S , are performed in place, without additional data movement. At the end of the parallel matrix product, the allocated memory for \hat{V} temporarily contains $S\hat{V}$ and is subsequently restored to its original signs, because \hat{V} is required thereafter.

Compared to the hermitian case, the pseudo-hermitian formulation introduces three sign-flip operations on the lower portions of tall-and-skinny matrices: one applied to \hat{V} prior to the matrix product, one applied to the intermediate result SW to obtain W , and one to restore \hat{V} . The sign-flip operations are required only when the search space is distributed within the column communicators. Since the multiplication of the search space distributed within the column communicators returns a matrix distributed within the row communicators, these three sign-flip operations are applied every two multiplication with H only. These sign-flip operations are computationally inexpensive and map efficiently to GPU architectures. Moreover, we also recall that the costs of the matrix products and the flip sign operations on \hat{V} decrease over successive iterations, as the number of converged eigenvector approximations increases and the effective dimension of the search subspace \hat{V} correspondingly shrinks.

7. Numerical tests. In this section, we test the extension of ChASE to pseudo-hermitian Hamiltonian. The numerical experiments are conducted using four pseudo-hermitian Hamiltonians arising from the Bethe-Salpeter equation and generated by the Yambo [15] code. Two matrices correspond to Hamiltonians emerging from the discretizations of a Silicon material (Si) with two different supercells, and have sizes 23,552 and 79,488, denoted as Si-23K and Si-79K respectively. Similarly, the remaining two matrices correspond to hamiltonians extracted from Molybdenum Disulfide (MoS₂) and have sizes 64,512 and 104,832, denoted as MoS₂-64K and MoS₂-104K respectively.

All the experiments are performed in double precision on the supercomputer JUWELS Booster located at Jülich Supercomputing Centre in Germany. The configuration of each compute node is 2 × 24 cores AMD EPYC 7402 CPUs @ 2.25 GHz (512GB Memory), 4×NVIDIA A100 GPU with 40 GB memory. The interconnect are 4×InfiniBand HDR (Connect-X6). The *theoretical peak performance* (TPP) of a single GPU is 19.5 TFLOP/s in double precision. The code is compiled with GCC 14.3.0 and CUDA 13. MPI library used is OpenMPI 5.0.8 with GPU-aware communication provided by UCX. Collective communications are handled through NCCL. BLAS/LAPACK libraries used are Intel MKL version 2025.2.0.

As a start, ChASE is used as a black-box solver, without incorporating problem-specific physical information. Accordingly, the size of the extra space is always set to $\mathbf{nex} := \mathbf{nev}$, and $\mathbf{nev} \in \{1\%, 2\%, 3\% \} \times n$. In practice, the parameter \mathbf{nex} can be tuned to improve convergence behavior and overall performance. For instance, our

experiments indicated that setting `nex` to $0.3 \times \text{nev}$ enables computing up to 5% of the spectrum of the large problem ($n = 104,832$) in only a few iterations. Automated selection of the upper-bound μ_{nevex} for the filter interval based on the approximation of the spectral density obtained via Lanczos at Line 2 in Algorithm 2.1 is a direction for further work. In the present study, we adopt an universal choice of `nex` - and set μ_{nevex} accordingly - in order to facilitate a consistent and transparent performance comparison across all test cases. For all experiments, the MPI process grid is configured to be as close to square as possible, which is optimal for ChASE performance.

7.1. Convergence Experiments. Figure 7.1 provides the number of iterations required by ChASE to solve the four pseudo-hermitian eigenproblems from Yambo, depending on the prescribed *residual error* tolerance and the variant of Rayleigh-Ritz. The maximal number of iterations depicted by the dashed red lines is set to `maxiter := 25`. First, we notice that the algorithmic variant of ChASE using the

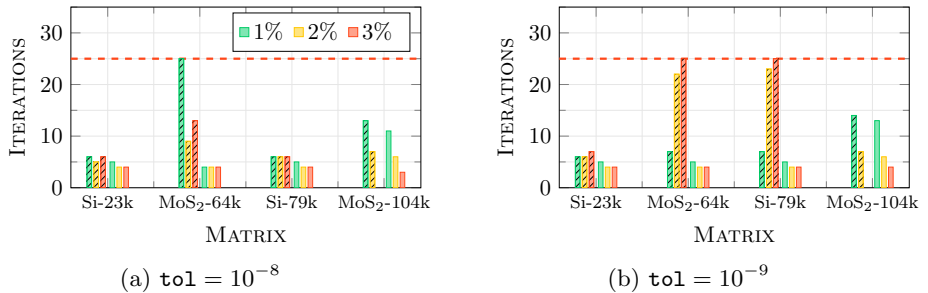


Fig. 7.1: Number of iterations with respect to the matrix size and residual tolerance - GEEV (dashed bars) vs. HEEVD (plain bars) - Internal failure of cuSOLVER GEEV in allocating the memory for MoS₂-104k with `nev = n × 3%`

hermitian spectral equivalent Rayleigh-Quotient (HEEVD - plain bars) always converges in less than 15 iterations. No failure of this variant has been noticed in this set of experiments. In addition, this variant converges faster than the *non-hermitian Rayleigh-Ritz* variant (GEEV - dashed bars). As expected, decreasing the tolerance generally leads to more iterations. Interestingly enough, ChASE with GEEV computes the 1% smallest eigenpairs of the $n = 64512$ sized Hamiltonian faster when requiring `tol = 10-9` in Figure 7.1b. This observation is probably due to the locking step at Line 10 in Algorithm 2.1 which extracts the converged eigenvectors from the search space. Subsequently, the search space gets more accurate as the locked eigenvectors achieve smaller residuals. One last observation is that the number of iterations does not increase with the increase of `nev`. The convergence even improves when increasing `nev` for the largest matrix. Indeed, since the value of the polynomial filter at λ_{nev} increases with the size `nex` of the extra space (see Figure 2.1) and that `nex = nev`, requesting more eigenpairs can lead to faster convergence. For this precise reason, enlarging the extra-space is especially important when the eigenvalues are packed. This feature is another motivation for future work to automate the tuning of `nex` based on the spectral density of state.

7.2. Performance Experiments. We evaluate the new ChASE solver on three pseudo-hermitian Hamiltonians in complex double precision: a *small* test case with

Si-23K matrix, a *medium* test case with MoS₂-64K matrix, and a *large* test case with MoS₂-104K matrix. Each experiment is repeated 5 times. In the figures, the lines represent the average over the 5 repetitions, while the shaded regions indicate the range from the minimum to the maximum values across these repetitions. The black lines represent the ideal scaling. The color scheme for each value of **nev** is the same as in Figure 7.1 (i.e., 1% in green, 2% in orange, 3% in red).

Matrix Name	nev = $n \times 1\%$	nev = $n \times 2\%$	nev = $n \times 3\%$
Si-23K	36.2	43.8	48.4
MoS ₂ -64K	78.2	78.1	78.2
MoS ₂ -104K	86.8	84.4	81.3

Table 7.1: Largest percentage of TPP occupied by ChASE for each matrix size with respect to **nev** on 16 GPUs over 5 repetitions

Our discussion includes a comparison with prior results from [16, section 3], which employed ELPA direct eigensolver (ELPA-one-stage solver) [19] and the SLEPc Lanczos based iterative method [1] in complex single precision for computing 100 extremal eigenpairs. Although difference in floating-point precision should be considered, the benchmarks in [16, figure 4] were performed on Leonardo Booster, which features the same GPU configuration as used in our experiments.

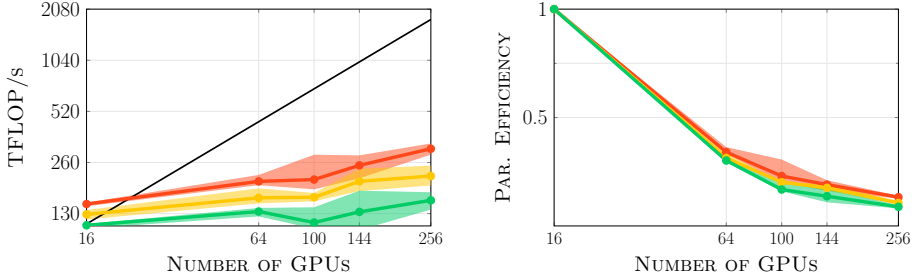


Fig. 7.2: Performance benchmark on a *small* matrix of size $n = 23,552$ - $\mathbf{nev} = 235, 471, 706$

Figure 7.2 shows that ChASE solves a small pseudo-hermitian eigenvalue problem of size $n = 23,552$ from 2 seconds for **nev** = 235 to 5 seconds for **nev** = 706 with 16 GPUs (i.e., 4 nodes on JUWELS-Booster). For reference, SLEPc computed 100 eigenpairs of a slightly smaller Hamiltonian ($n = 20,736$ ²) in 6 seconds using the same number of GPUs on Leonardo Booster, while ELPA completed the full diagonalization in under 1 minute. In addition, Table 7.1 indicates that ChASE sustains up to 48.4% of the TPP in this regime. As expected, strong scaling is limited by the relatively small local problem size: the size of the distributed local block of the Hamiltonian decreases from 5888 per GPU with 16 GPUs to 1472 per GPU with 256 GPUs.

For the medium-sized matrix ($n = 64,512$) illustrated in Figure 7.3, ChASE computes 1935 eigenpairs in less than 25 seconds using 256 GPUs, reaching approximately

²authors provides the size of the resonant A , i.e., $m = 10368$ in this example.

1 PFLOPS/s on average over the 5 repetitions. The sustained fraction of TPP decreases from more than 75% with 16 GPUs to slightly below 30% with 256 GPUs.

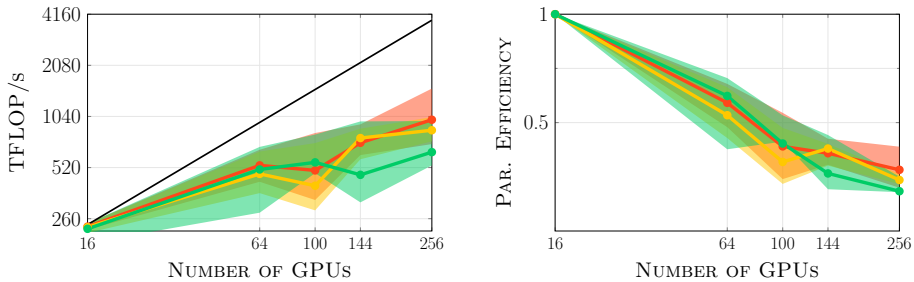


Fig. 7.3: Performance benchmark on a *medium* matrix of size $n = 64,512$ - $\mathbf{nev} = 645, 1290, 1935$

For the large matrix ($n = 104,832$), Figure 7.3 shows that ChASE achieves approximately 2 PFLOPS/s using 256 GPUs when computing the first thousand external eigenpairs in 35 seconds, corresponding to a sustained efficiency of 43.4% of TPP. For context, ELPA requires over 7 minutes to diagonalize a smaller matrix ($n = 72,576$) in single precision using 64 GPUs, while SLEPc extracts 100 eigenpairs in roughly 40 seconds ([16, figure 4]). In this regime, ChASE computes a larger number of eigenpairs for a larger problem size within a comparable time scale, illustrating its scalability on GPU-based architectures. A localized degradation is observed at 100 GPUs for $\mathbf{nev} = 2096$, which is attributed to numerical instability in the estimation of $\mu_{\mathbf{nevex}}$ with our pseudo-hermitian variant of Lanczos. This issue could be mitigated by adopting more advanced Lanczos strategies, such as those proposed in [1].

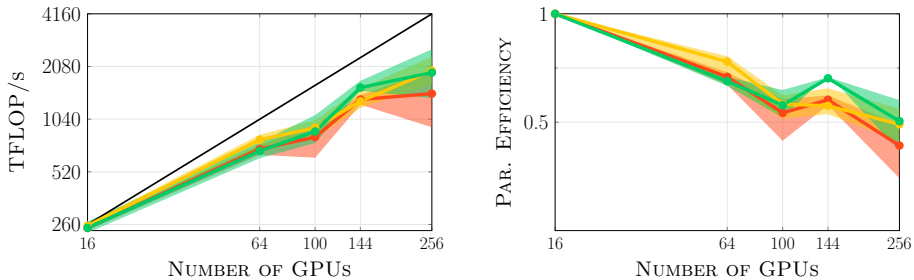


Fig. 7.4: Performance benchmark on a *large* matrix of size $n = 104,832$ - $\mathbf{nev} = 1048, 2096, 3144$

The pseudo-hermitian extension preserves the performance characteristics observed in the hermitian case. In [30], ChASE solved a hermitian problem of comparable size in complex double-precision (Hamiltonian size 115k, $\mathbf{nev} = 1000$ and $\mathbf{nex} = 400$), also on 64 JUWELS-Booster nodes (256 GPUs), converging in five iterations with a time-to-solution of approximately 8 seconds. Although not explicitly reported, the sustained performance can be estimated at approximately 2.1 PFLOPS, which is very close to the ~ 2 PFLOPS achieved in the present work. This indicates that the extension

to pseudo-hermitian problems maintains the high performance of ChASE. Overall, these experiments demonstrate that the ChASE expansion effectively exploits modern GPU systems for computing the smallest eigenpairs of large pseudo-hermitian matrices. This performance is primarily enabled by the Chebyshev filter, which relies heavily on highly optimized and scalable GEMM kernels and accounts for approximately 80% of the total computational workload.

For smaller matrices and when only a limited number of eigenpairs (e.g., at most around one hundred) are required, the results reported in [16] indicate that Lanczos-based solver from SLEPc can achieve time-to-solution comparable to that of ChASE. The same study also admits that extending Lanczos-based approaches to the computation of a substantially larger number of eigenpairs may encounter limitations related to numerical stability and robustness. In contrast, direct solvers such as ELPA are shown to be highly efficient for full diagonalization, but may incur unnecessary computational cost when only a few thousand eigenpairs are of interest. In this landscape, ChASE—while itself an iterative subspace method—naturally targets an intermediate regime, offering a scalable and robust alternative for problems where neither Lanczos-based solvers nor full diagonalization are ideally matched to the computational requirements.

8. Conclusion. Computing extreme eigenpairs of large excitonic Hamiltonians is critical in many Condensed Matter applications and especially for the simulation of optoelectronic properties of complex materials, where the pseudo-hermitian formulations plays an important role in preventing the limiting approximation of the reduction to hermitian form (TDA). While recent numerical libraries have improved support for pseudo-hermitian solvers, the efficient calculation of several thousand eigenpairs on modern heterogeneous architectures has remained an open question. This work extends ChASE to address this challenge by enabling the scalable computation of up to several thousand eigenpairs of large pseudo-hermitian Hamiltonians. The proposed Rayleigh-Ritz formulation, based on an implicit dual basis, yields a Rayleigh-Quotient that is spectrally equivalent to an hermitian matrix, and preserves quadratic convergence of the Ritz values, similarly to the hermitian case. By exploiting the numerical properties of the pseudo-hermitian Hamiltonian, the parallel implementation of the Chebyshev filter minimizes global communication and achieves competitive performance and strong scalability through extensive use of optimized GPU kernels. A rigorous numerical analysis is accompanied by a carefully designed set of experiments to demonstrate that ChASE provides an effective and scalable solution for large-scale pseudo-hermitian eigenproblems. Future work will focus on improving the Lanczos-based parameter selection for Chebyshev filtering and on automating the choice of the size of external searching subspace size, i.e., `nex`, via spectral density approximations.

REFERENCES

- [1] F. ALVARRUIZ, B. MELLADO-PINTO, AND J. E. ROMAN, *Variants of thick-restart Lanczos for the Bethe-Salpeter eigenvalue problem*, Mar. 2025.
- [2] F. BECHSTEDT, *Many-Body Approach to Electronic Excitations: Concepts and Applications*, vol. 181 of Springer Series in Solid-State Sciences, Springer Berlin Heidelberg, Berlin, Heidelberg, 2015.
- [3] P. BENNER, H. FASSBENDER, AND C. YANG, *Some remarks on the complex J-symmetric eigenproblem*, Linear Algebra and its Applications, 544 (2018), pp. 407–442.
- [4] L. S. BLACKFORD, J. CHOI, A. CLEARY, E. D’AZEVEDO, J. DEMMEL, I. DHILLON, J. DONGARRA, S. HAMMARLING, G. HENRY, A. PETITET, K. STANLEY, D. WALKER, AND R. C. WHALEY,

- ScalAPACK Users' Guide*, Society for Industrial and Applied Mathematics, Jan. 1997.
- [5] J. J. M. CUPPEN, *A divide and conquer method for the symmetric tridiagonal eigenproblem*, Numerische Mathematik, 36 (1980), pp. 177–195.
 - [6] M. GATES, A. ABDELFATTAH, K. AKBUDAK, M. AL FARHAN, R. ALOMAIRY, D. BIELICH, T. BURGESS, S. CAYROL, N. LINDQUIST, D. SUKKARI, AND A. YARKHAN, *Evolution of the SLATE linear algebra library*, The International Journal of High Performance Computing Applications, (2025), pp. 3–17.
 - [7] M. GRÜNING, A. MARINI, AND X. GONZE, *Exciton-Plasmon States in Nanoscale Materials: Breakdown of the Tamm-Danoff Approximation*, Nano Letters, 9 (2009), pp. 2820–2824.
 - [8] M. GRÜNING, A. MARINI, AND X. GONZE, *Implementation and testing of Lanczos-based algorithms for Random-Phase Approximation eigenproblems*, Computational Materials Science, 50 (2011), pp. 2148–2156.
 - [9] V. HERNANDEZ, J. E. ROMAN, AND V. VIDAL, *SLEPc: A scalable and flexible toolkit for the solution of eigenvalue problems*, ACM Transactions on Mathematical Software, 31 (2005), pp. 351–362.
 - [10] S. HIRATA AND M. HEAD-GORDON, *Time-dependent density functional theory within the tamm-danoff approximation*, Chemical Physics Letters, 314 (1999), pp. 291–299.
 - [11] R. A. HORN AND C. R. JOHNSON, *Topics in Matrix Analysis*, Cambridge University Press, 1 ed., Apr. 1991.
 - [12] T. IMAMURA, S. YAMADA, AND M. MACHIDA, *Development of a high performance eigensolver on the petascale next generation supercomputer system*, Progress in Nuclear Science and Technology, 2 (2011), pp. 643–650.
 - [13] L. LIN, Y. SAAD, AND C. YANG, *Approximating Spectral Densities of Large Matrices*, SIAM Review, 58 (2016), pp. 34–65.
 - [14] A. MAREK, V. BLUM, R. JOHANNI, V. HAVU, B. LANG, T. AUCKENTHALER, A. HEINECKE, H.-J. BUNGARTZ, AND H. LEDERER, *The ELPA library: scalable parallel eigenvalue solutions for electronic structure theory and computational science*, Journal of Physics: Condensed Matter, 26 (2014), p. 213201.
 - [15] A. MARINI, C. HOGAN, M. GRÜNING, AND D. VARSANO, *yambo: An ab initio tool for excited state calculations*, Computer Physics Communications, 180 (2009), pp. 1392–1403.
 - [16] P. MILEV, B. MELLADO-PINTO, M. NALABOTHULA, A. E. KUCUKALIC, F. ALVARRUIZ, E. RAMOS, L. WIRTZ, J. E. ROMAN, AND D. SANGALLI, *Performances in solving the Bethe-Salpeter equation with the Yambo code*, Apr. 2025.
 - [17] V. OLEVANO AND L. REINING, *Excitonic Effects on the Silicon Plasmon Resonance*, Physical Review Letters, 86 (2001), pp. 5962–5965.
 - [18] C. PENKE, *Efficient algorithms for solving structured Eigenvalue problems arising in the description of electronic excitations*, PhD thesis, Otto von Güricke Universität Magdeburg, 2022.
 - [19] C. PENKE, A. MAREK, C. VORWERK, C. DRAXL, AND P. BENNER, *High performance solution of skew-symmetric eigenvalue problems with applications in solving the Bethe-Salpeter eigenvalue problem*, Parallel Computing, 96 (2020), p. 102639.
 - [20] Y. SAAD, *Numerical Methods for Large Eigenvalue Problems: Revised Edition*, Society for Industrial and Applied Mathematics, Jan. 2011.
 - [21] E. E. SALPETER AND H. A. BETHE, *A Relativistic Equation for Bound-State Problems*, Physical Review, 84 (1951), pp. 1232–1242.
 - [22] M. SHAO, F. H. DA JORNADA, L. LIN, C. YANG, J. DESLIPPE, AND S. G. LOUIE, *A Structure Preserving Lanczos Algorithm for Computing the Optical Absorption Spectrum*, SIAM Journal on Matrix Analysis and Applications, 39 (2018), pp. 683–711.
 - [23] M. SHAO, F. H. DA JORNADA, C. YANG, J. DESLIPPE, AND S. G. LOUIE, *Structure preserving parallel algorithms for solving the Bethe-Salpeter eigenvalue problem*, Linear Algebra and its Applications, 488 (2016), pp. 148–167.
 - [24] G. W. STEWART, *Matrix Algorithms: Volume II: Eigensystems*, Society for Industrial and Applied Mathematics, Jan. 2001.
 - [25] A. TAL, M. MARSMAN, G. KRESSE, A. ANDERS, S. RODRIGUEZ, K. KIM, A. KALINKIN, A. ROMANENKO, M. NOACK, P. ATKINSON, AND S. MAINTZ, *Solving Millions of Eigenvectors in Large-Scale Quantum-Many-Body-Theory Computations*, in ISC High Performance 2024 Research Paper Proceedings (39th International Conference), May 2024, pp. 1–11.
 - [26] J. H. WILKINSON, *The algebraic eigenvalue problem*, Oxford University Press, Inc., USA, 1988.
 - [27] J. WINKELMANN, P. SPRINGER, AND E. D. NAPOLI, *ChASE: Chebyshev Accelerated Subspace Iteration Eigensolver for Sequences of Hermitian Eigenvalue Problems*, ACM Transactions on Mathematical Software, 45 (2019), pp. 1–34.
 - [28] K. WU AND H. SIMON, *Thick-Restart Lanczos Method for Large Symmetric Eigenvalue Prob-*

- lems, SIAM Journal on Matrix Analysis and Applications, 22 (2000), pp. 602–616.
- [29] X. WU, D. DAVIDOVIĆ, S. ACHILLES, AND E. DI NAPOLI, *Chase: a distributed hybrid cpu-gpu eigensolver for large-scale hermitian eigenvalue problems*, in Proceedings of the Platform for Advanced Scientific Computing Conference, PASC '22, New York, NY, USA, 2022, Association for Computing Machinery.
- [30] X. WU AND E. DI NAPOLI, *Advancing the distributed Multi-GPU ChASE library through algorithm optimization and NCCL library*, in Proceedings of the SC '23 Workshops of the International Conference on High Performance Computing, Network, Storage, and Analysis, Denver CO USA, Nov. 2023, ACM, pp. 1688–1696.

Appendix A. Proof for the field of values of H when SH is indefinite.

Proof. Decompose H into its hermitian and anti-hermitian parts:

$$(A.1) \quad \hat{H} := \frac{1}{2}(H + H^*), \quad \dot{H} := \frac{1}{2}(H - H^*), \quad H = \hat{H} + \dot{H}.$$

These matrices have the block forms

$$(A.2) \quad \hat{H} = \begin{bmatrix} A & 0 \\ 0 & -A^T \end{bmatrix}, \quad \dot{H} = \begin{bmatrix} 0 & B \\ -B^* & 0 \end{bmatrix}.$$

The field of values of H is defined by

$$(A.3) \quad \mathcal{F}(H) := \{ \quad \mathbf{x}^* H \mathbf{x} \quad | \quad \mathbf{x} \in \mathbb{C}^n \quad , \quad \|\mathbf{x}\|_2 = 1 \}.$$

Since \hat{H} is hermitian, its field of values is bounded by its smallest and largest eigenvalues, and its eigenvalues coincide with those of A and $-A$, yielding

$$(A.4) \quad \mathcal{F}(\hat{H}) = [-\rho(A), \rho(A)].$$

Multiplying by ι on \dot{H} yields the hermitian matrix $\iota\dot{H}$, whose eigenvalues are real. This transformation allows us to bound the spectrum of \dot{H} using standard hermitian arguments. Specifically, the eigenvalues of $\iota\dot{H}$ satisfy $\det(\iota\dot{H} - \lambda I) = 0$, which reduces to $\det(\lambda^2 I - B^* B) = 0$. Hence, the eigenvalues of $\iota\dot{H}$ are $\lambda_i(\iota\dot{H}) = \pm\sqrt{\lambda_i(B^* B)}$, and the eigenvalues of \dot{H} itself are purely imaginary, occurring in symmetric positive and negative pairs along the imaginary axis. The normal equation matrix $B^* B$ is also hermitian, so the bounds of $\mathcal{F}(\iota\dot{H})$ can be expressed as follows

$$(A.5) \quad \mathcal{F}(\iota\dot{H}) = [-\sqrt{\rho(B^* B)}, \sqrt{\rho(B^* B)}].$$

From [11, Chapter 1], we know that the field of values of the Hamiltonian H satisfies

$$(A.6) \quad \mathcal{F}(H) = \mathcal{F}(\hat{H} - \iota \times \iota\dot{H}) \subseteq \mathcal{F}(\hat{H}) - \iota\mathcal{F}(\iota\dot{H}).$$

Consequently, the eigenvalues λ_i of the full Hamiltonian H are enclosed in the complex plane

$$(A.7) \quad \operatorname{Re}(\lambda_i) \in [-\rho(A), \rho(A)] \quad \text{and} \quad \operatorname{Im}(\lambda_i) \in [-\sqrt{\rho(B^* B)}, \sqrt{\rho(B^* B)}]. \quad \square$$

Appendix B. Proof for the field of values of the Rayleigh-Quotient.

Proof. Since both matrices forming the Rayleigh-Quotient G in (5.16) are hermitian, their fields of values coincide with their spectral intervals. First, since Q^*SQ is assumed non-singular, its spectrum is symmetric with respect to zero, and we obtain

$$\mathcal{F}(Q^*SQ) \subset [-|\lambda_{\max}(Q^*SQ)|, -|\lambda_{\min}(Q^*SQ)|] \cup [|\lambda_{\min}(Q^*SQ)|, |\lambda_{\max}(Q^*SQ)|]$$

Second, the eigenvalues of Q^*SHQ interlace with those of SH , since Q is unitary. Therefore

$$(B.1) \quad \mathcal{F}(Q^*SHQ) \subset [\lambda_{\min}(SH), \rho(SH)].$$

By the result of [11, chapter 1], the Ritz values are contained in the field of values $\mathcal{F}(Q^*SHQ)/\mathcal{F}(Q^*SQ)$, which leads directly to (5.32). \square